Investigation of the Role of Membrane-Induced Conformational Change in the Function of the MinE Bacterial Cell Division Regulator

Laura J. McLeod

Thesis Submitted to the
Faculty of Graduate and Postdoctoral Studies
University of Ottawa
In partial fulfillment of the requirements for the
M. Sc. degree in the

Ottawa-Carleton Chemistry Institute

uOttawa

L'Université canadienne
Canada's university

Abstract

The Min system ensures that gram-negative bacteria undergo symmetric cell division. The three Min proteins, MinC, MinD, and MinE, display a dynamic pattern of subcellular organization on the inner cell membrane that directs division proteins to the mid-cell. This process is driven by the ATPase activity of MinD that is stimulated through its interactions with MinE. A recent structure of MinE in complex with MinD suggests that MinE undergoes a dramatic conformational change to allow MinD-binding residues to be released from the MinE hydrophobic core. However, this structure used a MinE mutant designed to favor this conformational change, raising questions regarding the mechanism by which wild-type MinE can undergo this transition *in vivo*. One potential scenario that might explain this structural change involves a recently discovered interaction between MinE and the membrane surface. To investigate the possibility that lipid binding could induce this structural transition in MinE, circular dichroism and enzyme kinetics studies were carried out. These studies were also done on MinE mutants designed to either eliminate membrane binding or induce the conformational change involved in MinD-binding. The results demonstrated that a membrane induced conformational change does occur, and requires the presence of a key lipid-binding region at the N-terminus. However, removal of this sequence failed to alter the kinetics of MinE-stimulated MinD-catalyzed ATP hydrolysis. Overall, our results provide a step forward in our understanding of the role of the interaction between MinE and the membrane in the Min system, but also highlight the need for additional investigation before this system might be used as a novel antibiotic target for pathogenic, gram-negative bacteria such as *Neisseria gonorrhoeae.*

Acknowledgements

First of all, I would like to thank my supervisor, Dr. Natalie Goto, for all of the support and inspiration through my time in the lab. Your feedback and encouragement have pushed me to ask better questions and become a more effective communicator. Under your direction I have come to appreciate the wonderful complexity that is Min and I have enjoyed being part of trying to piece it all together. I greatly appreciate all that you have contributed to bringing me to where I am today.

I would also like to thank the members of the Goto Lab for making the lab such a great place to work. In particular to Tabussom Qureshi not only for your experience and support but for sharing in all things ridiculous including but far from limited to the contingency plan, my tea addiction, and my growing knowledge of Bollywood; to Saud Ayed and Fatima Hafizi who have contributed greatly to this project, have helped me to see it from different angles, and can share in an appreciation of the fact that nothing with Min is ever straightforward; to Alex Foo and Jason Kwok, for being more helpful and courteous than I believed possible. Your polite-offs and nerd-alerts amuse me endlessly; to Dr. Allison Sherratt for the skills and consultations, which have carried me through this project; and to Noreen Singh for taking on this project with enthusiasm. Additional thanks go out to Mirka Strmiskova for her consults on mutagenesis, the Keillor and Scaiano labs for the use of their CD spectropolarimeters, the Moon lab for the use of their spectrometer and the Boddy lab for the use of their mass spectrometer.

Finally I would like to thank my family. Mom, Dad, and Kate for their endless support and encouragement and Adam for his support and occasionally necessary reminders that it is all going to be ok.

Table of Contents

List of Abbreviations

BCA	bicinchoninic acid
BLAST	basic local alignment search tool
CD	circular dichroism
ddH_2O	double distilled water
DOPG	1,2-dioleoyl-*sn*-glycero-3-[phosphor-*rac*-(1-glycerol)]
E. coli	*Escherichia coli*
GFP	green fluorescent protein
LB	Luria-Bertani
LUVs	large unilamellar vesicles
MALDI	matrix assisted laser desorption ionization
Min-Ec	Min proteins from *E. coli*
Min-Ng	Min proteins from *N. gonorrhoeae*
MTS	membrane targeting sequence
N. gonorrhoeae	*Neisseria gonorrhoeae*
OD	optical density
PAGE	polyacrylamide gel electrophoresis
QCM	quartz crystal microbalance
SDS	sodium dodecyl sulfate
TIRF	total internal reflection fluorescence
TSD	topological specificity domain
WT	wild-type

List of Figures

List of Tables

Chapter 1: Introduction

1.1 The Rise of Antibacterial Resistance

Since the discovery of penicillin by Alexander Fleming in 1929 our repertoire of antimicrobial agents has expanded, but so too has the ability of pathogens to evade them (1, 2). Populations of *Neisseria gonorrhoeae (N. gonorrhoeae)*, the gram-negative bacterium responsible for the sexually transmitted infection Gonorrhea, once susceptible to a wide range of antibiotics including penicillin, have become resistant to such therapies (2, 3). In April 2013 the Ontario Public Health Authority once again altered its treatment guidelines for Gonorrhea in response to growing resistance to the first line treatment, third-generation cephalosporins. The new guidelines recommend a combination treatment of cephalosporins with azithromycin or doxycycline with the intent that combination therapy has potential to slow the development of resistance (3). While this new approach may prove effective for the time being, the identification of a new target will be essential for treatment of these infections in the future. The Min system, which regulates cell division in gram-negative bacteria, but has no human homologue, provides an attractive candidate for this new target since Min system disruption in *N. gonorrhoeae* causes cell lysis (4). However, the Min system has proved to be complex, and a more complete understanding of the nuances of the system will be required before inhibition will be possible.

1.2 Selecting the Division Site: Nucleoid Occlusion and Min

In order to promote the survival of subsequent generations, bacteria divide into daughter cells of approximately equal size, ensuring equal distribution of genetic information. Division occurs through binary fission, which is initiated by the polymerization of FtsZ, a homologue of tubulin (5). The polymerization of FtsZ forms the foundation upon which the other division proteins sequentially assemble to form the Z-ring, which drives cell division (6). Being the first step in cell septation, the polymerization and localization of FtsZ is tightly regulated to ensure division events occur exclusively at the mid-cell point.

Two complementary processes regulate selection of the optimal division site in gram-negative bacteria: the nucleoid occlusion system and the Min system. While the presence of the nucleoid occlusion system safeguards against DNA bisection and allows for optimal division plane selection, it is not required for successful division (7). Its absence can be compensated for by the Min system, which prevents division events at the cell poles. In contrast, when the Min system is knocked out, enucleated mini-cells arise in the bacterial population as shown for *Escherichia coli* (*E. coli*) cells in Figure 1. Mini-cells arise when cell septation occurs at one of the cell poles, forming one mini-cell and one longer rod-shaped cell containing duplicated chromosomal material (8).
The three proteins comprising the Min system, namely MinC, MinD, and MinE, prevent the formation of mini-cells through a coordinated cycle of interactions (9). In this cycle, MinC acts as an inhibitor of cell division, as suggested by the observation of a filamentous phenotype when both MinC and MinD were overexpressed in *E. coli* cells (Fig. 1.1C)(8). It was subsequently shown in this mutant that MinC localizes to the

membrane through interactions with membrane-bound MinD, and that in this state it can bind directly to FtsZ, inhibiting the polymerization required for Z-ring formation (10-13). When MinE is reintroduced to the system regular cell division is restored, indicating that it is a regulator of this MinCD-mediated inhibition (8). The mechanism by which MinE dictates the localization of the other two Min proteins is the focus of this thesis.

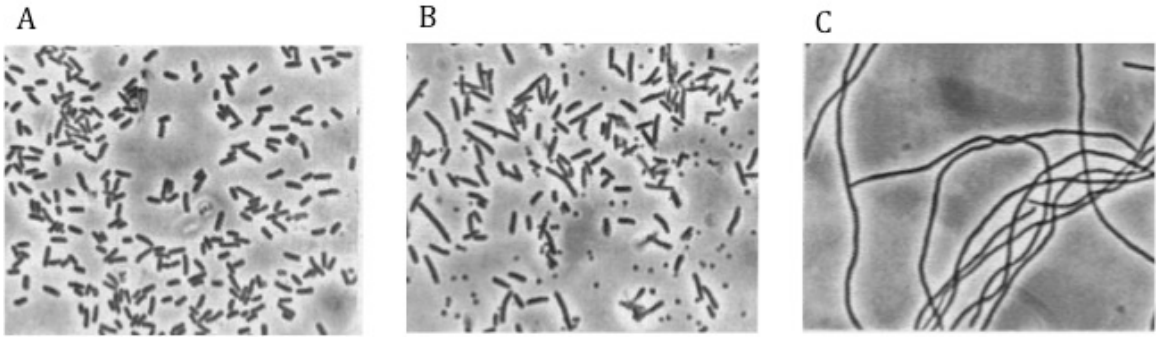

Figure 1.1: Importance of the Min system for *E. coli* division. A) Phase contrast microscopy images of wild-type (WT) *E. coli* showing uniform rod-shaped morphology. B) Morphology of *E. coli min* knockout mutant showing mini-cells and elongated cells as a result of polar division events. C) Overexpression of MinC and MinD in the *min* knockout strain produces filamentous cells. Figure from De Boer et al. 1989, Cell, reprinted with permission (appendix A2) (8).

1.3 The Min System: Oscillation

Proper localization of MinC within the cell is essential to ensure that division occurs only at the midpoint. Interplay between MinD and MinE dictates the localization of MinC by establishing a pole-to-pole oscillation of Min proteins (9). This oscillation was first observed in *E. coli* cells by fluorescence microscopy in studies of Min fusions with green fluorescent protein (GFP) (10, 11, 14). As shown in an example of this oscillation in Figure 1.2, the cycle starts with MinD localized to the membrane at one

cell pole. Approximately 10 seconds later the fluorescence becomes distributed throughout the cell body, before becoming concentrated at the opposite pole by the 20 second time point. The cycle then continues, with the MinD again accumulating in the original pole (14). This oscillation pattern from pole to pole is also seen for MinC, which co-localizes with MinD throughout the cycle (10, 11). As a result the membrane-bound MinCD complex has a time-averaged concentration that is highest at the cell poles, inhibiting formation of the cell septum at these sites. However, MinC is not required to observe oscillation, with MinE and MinD being the only components needed for this to occur (10).

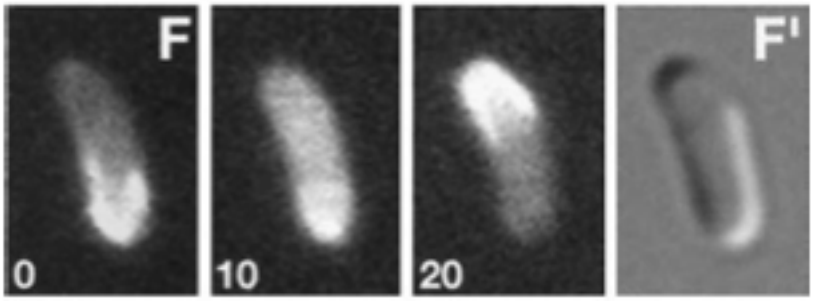

Figure 1.2: Pole to pole oscillation of GFP-labeled MinD. Fluorescence micrographs of *E. coli* expressing GFP-labeled MinD. At time zero (far left) MinD was concentrated at one pole of the cell. After 10 seconds the fluorescence is distributed throughout the cell body. By t=20 seconds the GFP-MinD has accumulated in the opposite pole. The panel on the far right shows the interference contrast micrograph of the same cell. Figure from Raskin et al. 1999, PNAS reprinted with permission (appendix A2) (14).

Fluorescently tagged MinE has also been shown to form a subcellular structure that oscillates from pole to pole. In this case, a concentrated annulus of MinE, known as the E-ring, forms at the growing edge of the MinD-rich zone as it extends towards the mid-cell. Once at mid-cell the E-ring appears to stimulate the decay of the MinD-rich

zone back towards the pole from which it had originated (15-17). While a large portion of cellular MinE is present in the E-ring, it has also been shown to be distributed throughout the MinD-rich zone, albeit at lower concentrations than is seen in the E-ring (15-17).

The dynamic self-organization of Min proteins on the subcellular scale has been recapitulated by *in vitro* experiments with fluorescent-labeled Min proteins on planar lipid bilayer surfaces using both confocal and total internal reflection fluorescence (TIRF) microscopy. In the presence of ATP, MinD and MinE together form wave-like patterns characterized by alternating bands of MinD, MinE, and free lipid that move across the lipid surface (18, 19). The formation of these dynamic higher-order structures on planar surfaces indicates that *in vivo* oscillation is not driven by spatial indicators in the cell, but is instead a manifestation of the interplay between MinD and MinE interactions. This can be observed in kymographs showing how position-dependent fluorescence intensities measured by TIRF change over time (Figure 1.3A)(19). These kymographs show that MinD forms a concentrated band with highest intensity near the middle of the wave. In contrast, the concentration of MinE increases slowly over the width of the wave, then rapidly spikes once the most concentrated region of MinD has passed. MinE and MinD then rapidly dissociate from the membrane at the trailing edge of the wave, although the burst of MinE dissociation begins a little later than MinD, but with a faster rate (Fig. 1.3B).

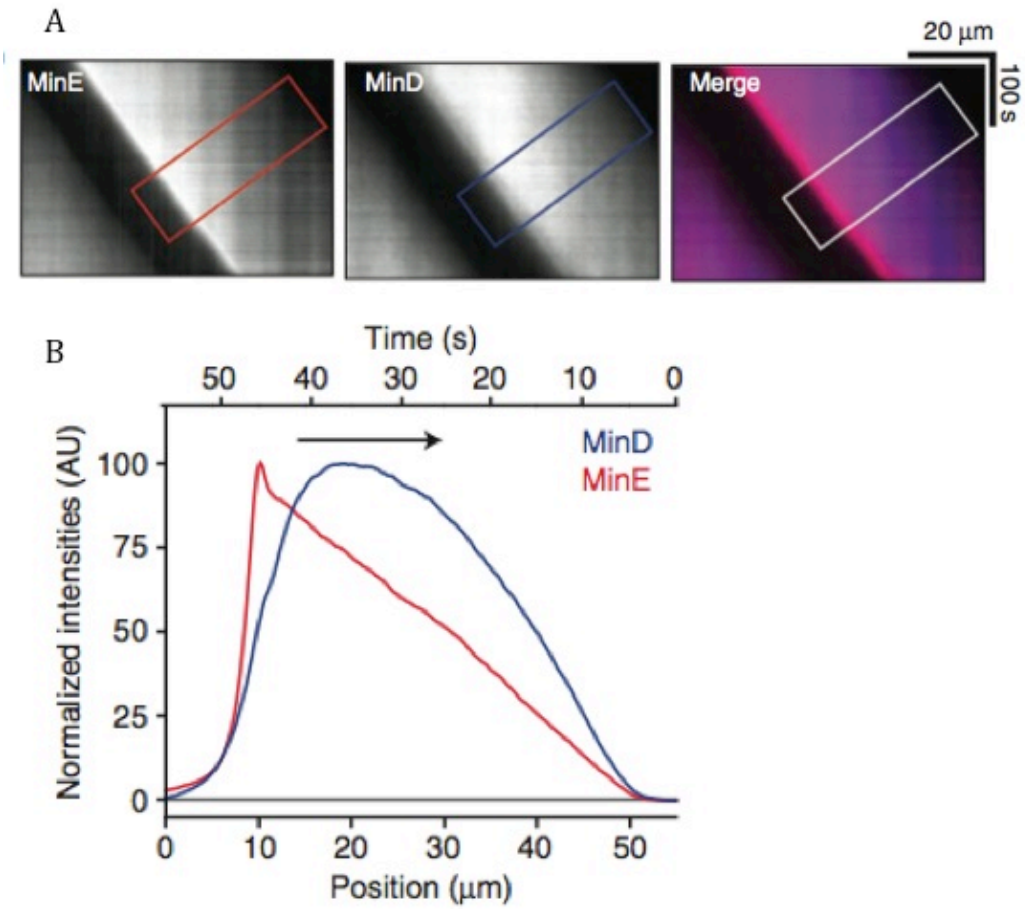

Figure 1.3: Propagation of Min waves on supported lipid bilayers. A) Kymographs of wave sections from TIRF micrographs detecting tagged MinE or MinD. The adjacent panel shows the merged kymographs where MinD is represented in blue, MinE in pink, and overlapping signals in purple. B) Fluorescence intensity profiles obtained from kymograph sections in the red or blue boxes for MinE and MinD respectively. MinD density increases approximately linearly from the leading edge of the wave, plateaus at the center and then decreases with a slightly larger slope. MinE accumulates much more slowly than MinD with a sharp maximum at the trailing edge of the wave followed by a rapid intensity decrease. The MinE maximum occurs just after the end of the MinD plateau. Figure from Loose et al. 2011, Nature Structural and Molecular Biology reprinted with permission (appendix A2) (19).

1.4 Interactions of Min Proteins

To further understand the oscillation observed *in vivo*, and the dynamic pattern formation seen *in vitro*, a number of biochemical studies investigating the interactions between Min proteins have been performed (9).

The results of these studies can be summarized in an interaction cycle between Min proteins and the membrane (see Fig. 1.4). This cycle starts with MinD in the cytoplasm in a monomeric ADP-bound state that can undergo nucleotide exchange with ATP (20-22). This causes dimerization of MinD, and a conformational change that allows an interaction between its C-terminal amphipathic helix and the inner membrane surface (20-25). This interaction has been shown to be more favorable when negatively charged lipids are present in the membrane (26). These membrane-bound dimers can then recruit MinC, forming the MinCD complex. MinE, having a higher affinity for a binding site on MinD that overlaps the MinC-binding site, can displace MinC from the complex (27-29). MinE binding also stimulates the ATPase activity of MinD; *in vitro* this stimulation increases the rate of ATP hydrolysis by 10-fold (28, 30, 31). ATP hydrolysis then regenerates cytoplasmic monomeric MinD, allowing the cycle to begin again.

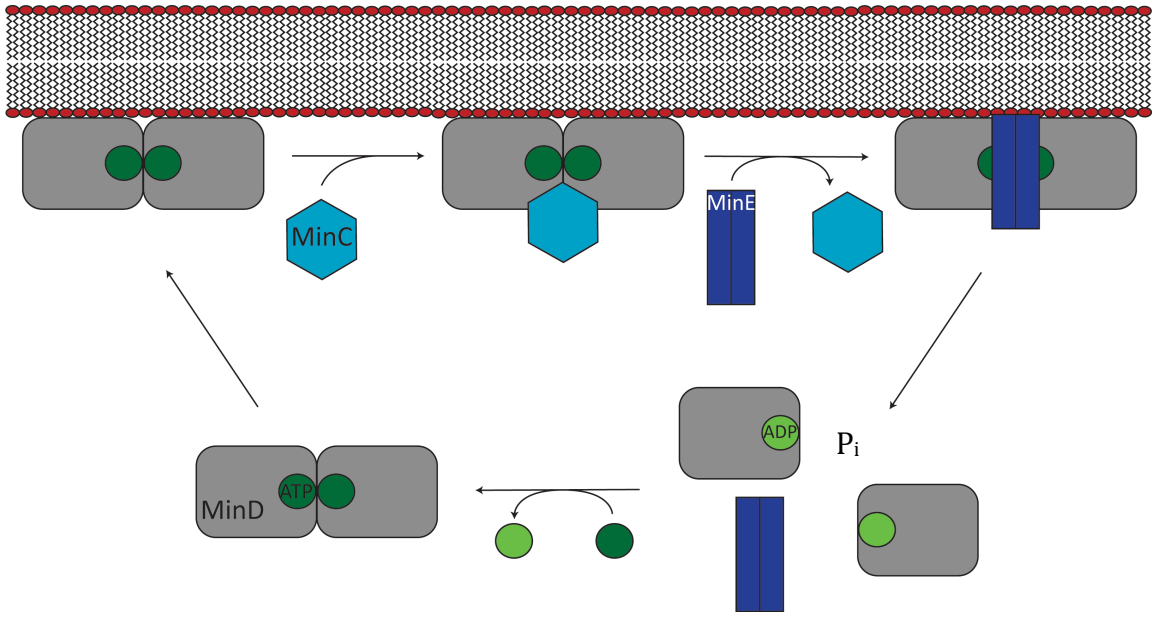

Figure 1.4: Molecular Interactions between Min proteins. Starting at the bottom left MinD (grey) bound to ATP (dark green circle) forms a dimer, which targets to the membrane. MinC (light blue hexagon) interacts with this membrane-bound dimer, forming the MinCD complex, which inhibits FtsZ polymerization. MinE (dark blue rectangles) can displace MinC from the complex and bind to MinD. MinE stimulates MinD-catalyzed ATP hydrolysis, which causes the release of MinD from the membrane into a momeric ADP-bound state. MinD then undergoes nucleotide exchange and the cycle continues (9).

Some link between these biochemically elucidated interactions and the patterns observed on planar lipid bilayers were recently provided by photo-bleaching and single-molecule tracking TIRF experiments with fluorescent labeled Min proteins (19). Results from these experiments showed that both MinD and MinE enter the wave from the leading edge, and that MinE spends significantly more time within the wave than MinD. This suggested that MinE likely interacts with MinD and stimulates its dissociation from the membrane without necessarily being released from its own interaction with the superstructure. This raised the possibility that one membrane-bound MinE protein could bind to and stimulate the dissociation of multiple copies of MinD before dissociating from the wave itself. This could explain the observed increase

in the ratio of MinE to MinD during the build-up of the wave (Fig. 1.3B). Once the MinD to MinE ratio reaches a threshold level, which was measured to be approximately one, coordinated dissociation of MinD is initiated and MinE density rapidly decreases. This model of Min wave propagation is known as the rapid rebinding model (19), since MinE is suggested to persist in its association through a rapid re-association with a new MinD binding partner after release from its previous interaction partner. This phenomenon is potentially mediated by direct interactions between MinE and the membrane (19, 32, 33).

1.5 Relationship Between *E. coli* and *N. gonorrhoeae* Min Proteins

It is important to note that the majority of work that has been done on the Min system has focused on Min proteins from the *E. coli* system (Min-Ec), while our studies focus on Min proteins from the more clinically relevant *N. gonorrhoeae* (Min-Ng). However, protein sequence alignment, with the basic local alignment search tool (BLAST), of Min sequences show a high degree of sequence similarity between proteins from the two species with 75% and 42% sequence identity for MinD and MinE, respectively (34, 35). This high level of sequence homology suggests that the two proteins should also have very similar structures, and work via similar mechanisms. This is supported by complementation and overexpression studies in an *E. coli* MinD knockout strain, which showed that MinD-Ng could rescue division (22). Also, overexpression of MinD-Ng in this *E. coli* strain produced filament cells, indicating MinD-Ng behaves identically to MinD-Ec (22). Further support for the functional similarity between the two Min proteins was provided by the observation that

overexpressed GFP-labeled MinD-Ng and MinE-Ng can oscillate in an *E. coli min* knockout strain. In addition, substitution of either of the two Min-Ng proteins for their Min-Ec analogue preserved this oscillation, indicating that the MinD-MinE interaction is the same across the two species (36). Overall, the high degree of sequence identity and demonstrated interchangeability of Min proteins between *E. coli* and *N. gonorrhoeae* provide strong evidence that the findings from one system are likely to be general across the Min family.

1.6 MinD Structure and Interactions

When a high-resolution structure of the MinD dimer from *E. coli* became available many details of the driving forces behind its interactions were revealed. In this structure a hydrolysis deficient mutant was used that could still interact with both MinE and MinC (D40A) (29). This structure showed that MinD co-ordinates ATP with its Walker A motif characterized by the sequence X<u>K</u>GGXXK[T/S], a motif that is conserved across the MinD family (20). The signature lysine (underlined), K11 in the case of the *E. coli* MinD, is a unique feature of the Walker A motif in the MinD family, and was revealed to play an essential role in formation of the MinD dimer (29). Each subunit in the dimer contains a cavity that binds to one molecule of ATP, but also makes contacts across the dimer to the ATP molecule bound to the other subunit. The signature lysine appears to be one of the key residues participating in this inter-subunit interaction (29).

Interactions between MinD and either MinC or MinE require ATP, indicating that they interact with the dimeric form of MinD (27, 28). Residues in MinD important for

these interactions have been identified in a series of mutagenesis studies, and have been mapped on the structure of the MinD dimer in Figure 1.5 (29). A cluster of residues was shown to be important for binding both MinC and MinE, consistent with the ability of MinE to displace MinC. In addition, MinE-binding residues localize to a cleft formed between the two subunits in the dimer, explaining the requirement of MinD dimerization for the MinE interaction (29).

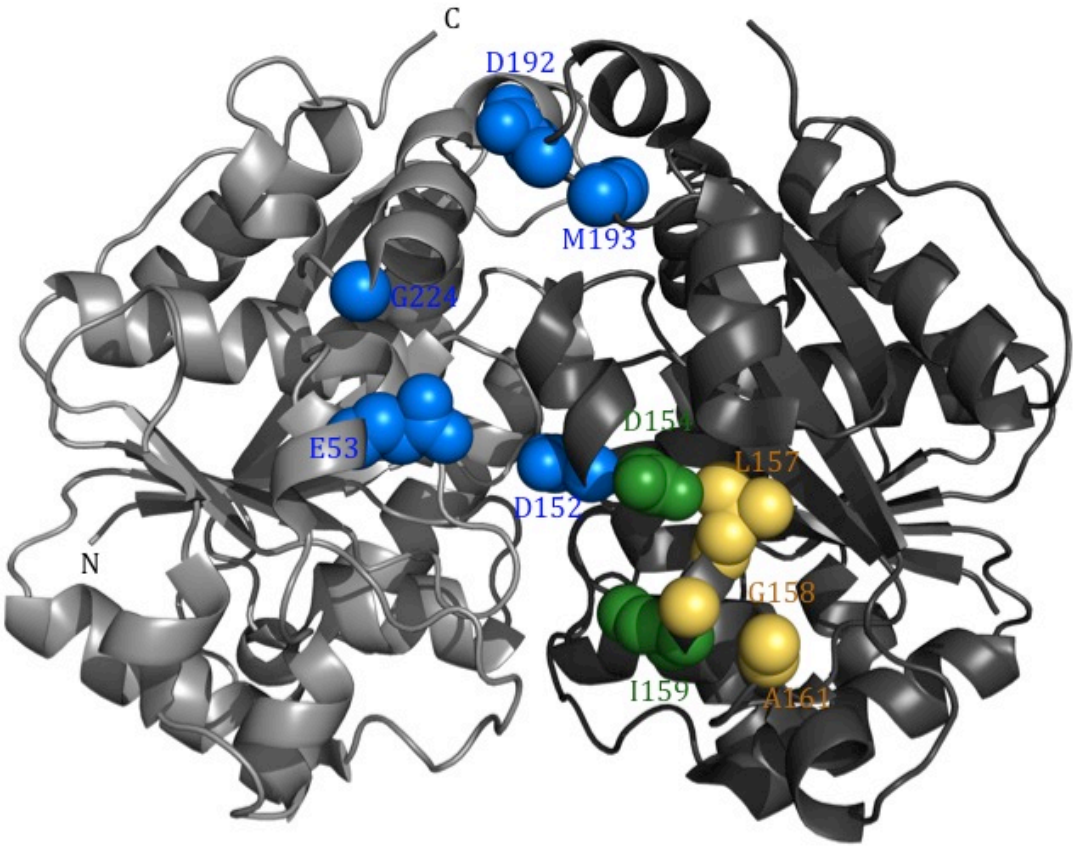

Figure 1.5: Crystal structure of the *E. coli* MinD dimer (PDB ID 3Q9L). Side chains of residues important for MinE binding (E53, D152, D192, M193, and G224) are shown in blue. Those important for binding both MinE and MinC, (D154, I159), are shown in green. Residues required for interactions with MinC are shown in yellow (L157, G158, A161) (29).

1.7 Full Length MinE Structure Reveals Sequestration of MinD Binding Residues

Early studies on truncation mutations of MinE gave rise to the assignment of two functional domains; namely, the anti-MinCD domain comprised of residues 1-30, and the topological specificity domain (TSD) comprised of residues 31-88 (37). This assignment was supported by yeast 3-hybrid studies showing that the anti-MinCD domain alone could interact with MinD to disrupt the MinCD complex (38). Meanwhile, the TSD was shown to produce mini-cells when overexpressed in wild-type (WT) *E. coli* cells, suggesting that it is required to direct the oscillation of MinD (37). The functional independence of these two domains appeared to coincide with structural independence, since a truncated mutant containing only residues 32 to 88 (MinE32-88) formed a stable dimeric structure that could be determined by solution NMR (Fig. 1.6)(39). This dimer is composed of a four-stranded β-sheet packed against a pair of α-helices. The dimer interface is extensive, being formed between a central pair of β-strands (residues 72-81) and the two helices.

Solution NMR studies of the first 22 residues of MinE were also done, and showed a largely unstructured conformation with some tendency to sample helical configurations (40). Based on this observation, along with site-directed mutagenesis results identifying residues important for the interaction with MinD, it was suggested that the anti-MinCD domain bound MinD in a helical conformation. In particular, helical wheel projections of the anti-MinCD domain showed these MinD binding residues would localize to one side of the helix (38).

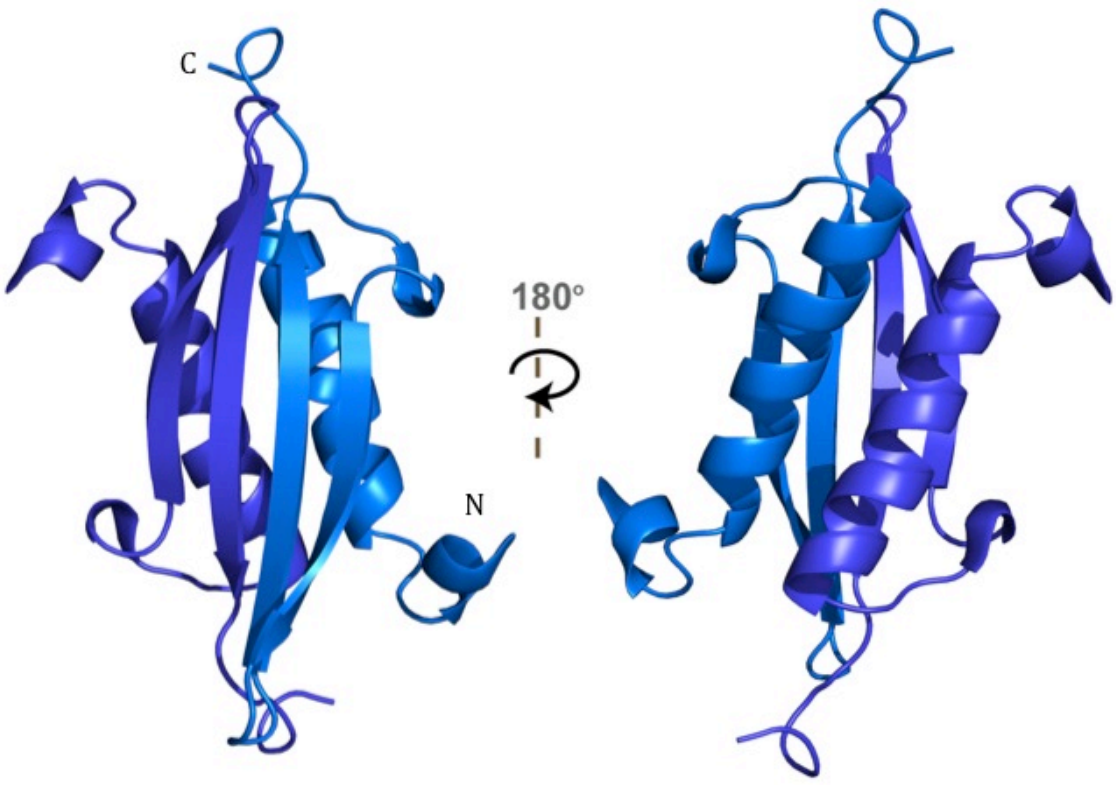

Figure 1.6: Solution NMR structure of the topological specificity domain of MinE. The two subunits are shown with different shades of blue. PDB ID 1EV0 (39).

Subsequent structural studies on the full-length MinE raised questions regarding this structural model, with solution NMR suggesting that the anti-MinCD domain was actually interacting with the TSD (41). Subsequent determination of the full-length solution NMR structure of MinE from *N. gonorrhoeae* confirmed this picture, with the anti-MinCD domain forming a central part of a six-stranded β-sheet (Fig. 1.7)(31). Most remarkably, the inter-molecular interface was different from that observed for the isolated TSD, with residues 21-30 forming a central β-strand in the dimer, which was involved in inter-molecular hydrogen bonding.

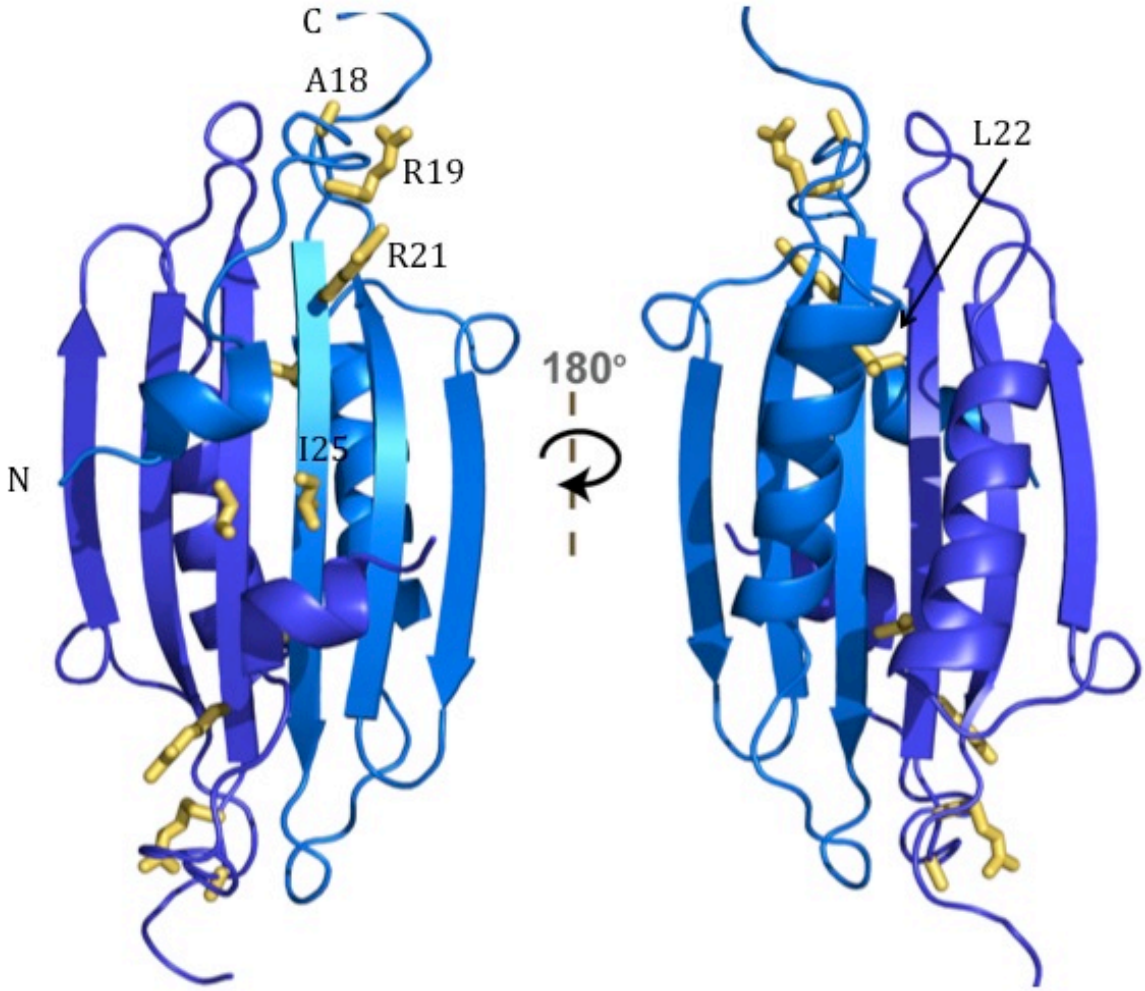

Figure 1.7: MinD binding residues localize to the dimer interface of the full-length, solution NMR structure of MinE from *N. gonorrhoeae* (PDB ID 2KXO). Residues A18, R19, R21, L22, and I25, shown as yellow sticks, were shown to be required for maximal stimulation of MinD activity (31, 38). Note that Leu22 and Ile25 reside within solvent inaccessible regions of the dimer interface.

One of the surprising features of this structure is that many residues that were shown to be important for direct interactions between MinD and MinE were not solvent-accessible, but were buried at the core of the dimeric interface. When these residues were mutated in a peptide model of MinE containing residues 1-27, stimulation of MinD activity *in vitro* was significantly reduced (31). These results were consistent with previous yeast 3-hybrid studies using MinE residues 1-30, which

showed a reduced ability to disrupt the MinCD complex upon mutation of key residues (38). The location of many of these residues within the dimer interface raises questions regarding how MinD can gain access to bind them.

1.8 Accessing MinD-Binding Residues

The solvent-inaccessible location of important MinD binding residues in the full-length MinE structure raised the possibility that the active form of MinE was not the dimer, but rather a monomeric form that would expose these residues for binding. However, NMR amide exchange experiments indicated that the interior β-sheets were highly protected from solvent exchange, suggesting that hydrogen bonding across the dimer is very stable (31). The high stability of the dimer was further substantiated by analytical ultracentrifugation studies that did not detect any monomeric species, even at micromolar concentrations (31). Moreover, crosslinking studies with cysteine mutants showed that covalently linked dimers retained full activity (42), demonstrating that it is the dimeric state of MinE that interacts with MinD.

Since it appeared that dimeric MinE is the active species responsible for MinD activation, an alternative explanation was required to account for the ability of MinD to bind to MinE residues that are solvent inaccessible. Specifically, it was suggested that the MinE structure undergoes a significant conformational change.

Strong evidence that MinE could undergo a dramatic conformational change was demonstrated by a crystal structure published by Park et al. in 2011 (33). In this low-resolution structure, MinE containing the I24N mutation, and missing the first 11 amino

acids was captured in complex with a hydrolysis deficient MinD mutant (D40A) that was also missing its membrane binding domain. Figure 1.8 shows the full-length structure of MinE (A) next to the crystal structure of the MinDE complex (B), highlighting the dramatic differences in the MinE structure. Specifically, instead of the 6-β-stranded structure seen in free MinE, the MinD-bound state has a 4-β-stranded structure with residues 72-81 making dimer contacts between sheets, as was observed with the structure of the TSD (33, 39). In this conformation the anti-MinCD domain of MinE is free to bind to MinD as a helix, indicating that the helical tendencies of the free anti-MinCD domain can be stabilized by its interaction with MinD (33, 40).

These dramatically different structures suggest a mechanism by which MinD gains access to buried residues. However, it is likely that the 4-stranded structure was induced by the introduction of a polar Asn into the hydrophobic core of the dimeric interface by the substitution of Ile-24. Since WT MinE would normally have a stable dimeric interaction that would make this conformational transition very unfavorable, it is still not clear how this conformational change could be triggered *in vivo*. However, one possibility, which is explored in this thesis, is that direct interactions between MinE and the membrane could be responsible for driving this conformational change.

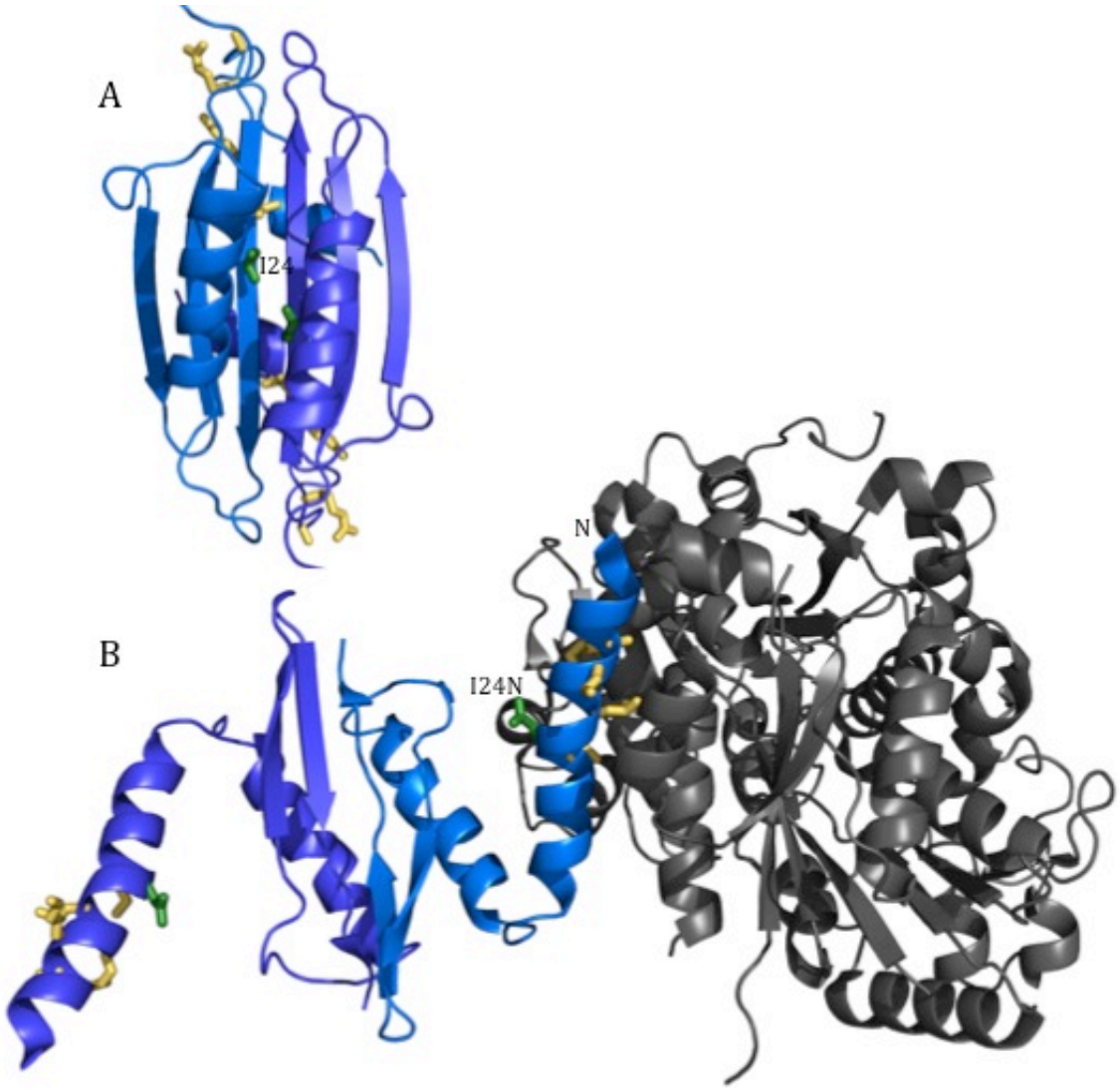

Figure 1.8: Two dramatically different conformations of MinE. A) Solution NMR structure of full length, *N. gonorrhoeae* MinE (blue) with residue I24 highlighted in green. Side chains of other MinD-binding residues are shown in yellow. PDB ID 2KXO (31) B) Crystal structure of residues 12-88 from the *E. coli* MinE-I24N mutant (blue) in complex with the ATP-hydrolysis deficient D40A mutant of MinD (grey) PDB ID 3R9J (33).

1.9 MinE and the Membrane Targeting Sequence

MinE has long been known to target to the membrane through an interaction with MinD (16), however recent vesicle sedimentation studies have demonstrated that

MinE can independently support an association with lipid membranes (32). Furthermore, these studies showed that the N-terminal fragment containing the first 31 residues of MinE (MinE1-31) bound with greater affinity, with 85% being found in the lipid pellet compared to only 15% of the WT. Increasing the ionic strength decreased the affinity of MinE for the lipids with association being completely undetectable above 200 mM NaCl, indicating that this effect is mediated by electrostatic interactions. Based on the preference of MinE to bind to negatively charged lipids, clusters of conserved basic residues within the first 31 residues of MinE were identified for investigation: C1 (Arg-10, Lys-11, Lys-12), C2 (Lys-19, Arg-21) and C3 (Arg-29, Arg-30, Arg-31). These clusters of residues were mutated to either Glu or Asp on MinE1-31 and expressed in a *min* knockout strain of *E. coli.* These cells were fractionated, and the C2 and C3 MinE mutants were both found to localize to the membrane fraction while the C1 MinE mutant remained cytoplasmic. This suggested that the residues mutated in the C1 mutant are essential for mediating the interaction between MinE and the membrane (32). Fluorescence microscopy experiments on these mutants expressed in *E. coli min*$^-$ cells confirmed these localization results, with the C1 mutant showing a fluorescence intensity profile suggestive of a cytoplasmic distribution, while C2 and C3 mutants had profiles that suggested some association with the membrane (32).

Fluorescence microscopy was also used to characterize the membrane localization properties of MinE-I24N, the mutant that likely adopts a 4-stranded conformation similar to that seen in the MinDE complex structure (33). Unlike WT MinE, this mutant localizes strongly to the membrane in *min*$^-$ *E. coli* (16, 33). Moreover, if additional mutations were introduced to the I24N variant to substitute hydrophobic

residues in the N-terminal amphipathic helix (i.e. Leu-3, Leu-4, Phe-6, or Phe-7) with a negatively charged Asp residue, a cytoplasmic localization was observed (33). This gave rise to the assignment of the N-terminal 13 residues as the membrane-targeting sequence (MTS, Fig. 1.9).

Interestingly, ^{15}N spin relaxation measurements showed the presence of microsecond to millisecond timescale motions for the N-terminal helix, consistent with the presence of conformational exchange where this N-terminal helix dissociates from the main body of the protein, thereby increasing its accessibility for intermolecular interactions (31). This is of particular interest in the context of circular dichroism (CD) studies previously carried out in the Goto lab, which showed that MinE undergoes a conformational change in the presence of lipids (43). This suggests that interactions with lipid membranes may help to drive the conversion of the 6-stranded structure seen in the absence of MinD to the 4-stranded structure observed in the MinDE complex, a possibility that will be investigated in this thesis.

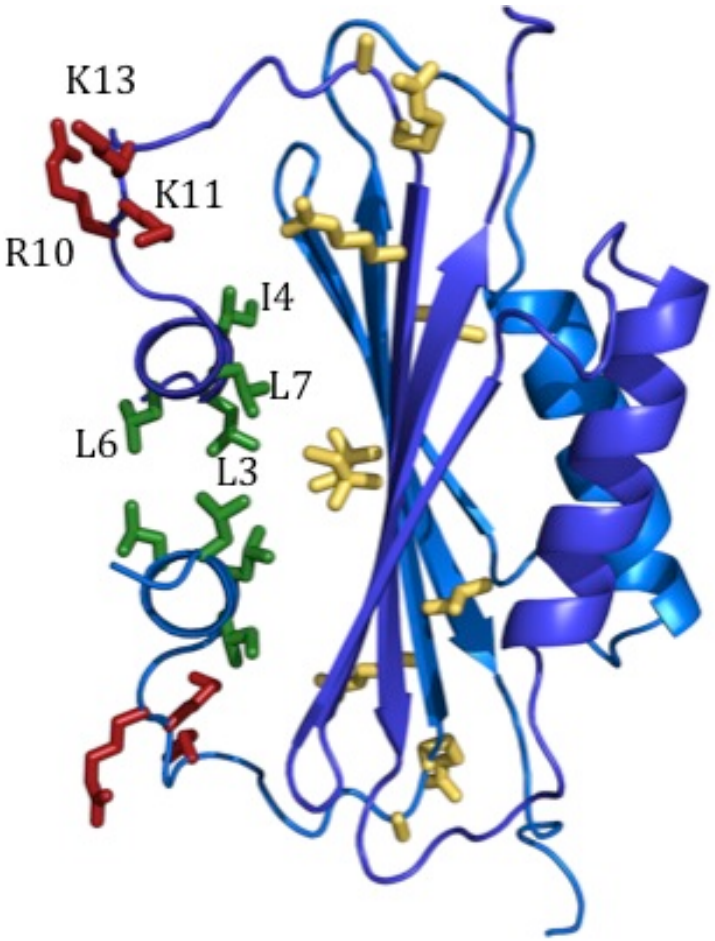

Figure 1.9: Residues important for MinE interactions with lipid membranes. MinE-Ng structure (PDB ID 2KXO (31)) highlighting hydrophobic residues (green), identified by Park et al. 2011, and positively charged residues (red), identified by Hseish et al. 2010, implicated in membrane targeting of MinE (32, 33).

1.10 Thesis Goals

This work seeks to characterize the interaction between MinE and the membrane and the impact that this interaction has on both the structural and functional characteristics of MinE. Previous studies in the Goto lab using CD spectroscopy demonstrated that MinE undergoes a conformational change in the

presence of lipids (43). In this work a more quantitative analysis of the secondary structure of the lipid-bound and free states of MinE were performed, and the affinity of MinE for lipids was measured.

In addition to these structural studies, we also wanted to determine the functional role of the lipid induced conformational change observed by CD. In particular, is this conformational change required to facilitate the interaction between MinD and MinE? In order to address this question we used measurements of MinE-stimulated MinD-catalyzed ATP hydrolysis kinetics. For this purpose, mutations intended to induce the 4-stranded structure of MinE either in the presence or absence of the first 12 N-terminal residues were generated, and tested for their ability to activate MinD.

Taken together, results from these studies should bring us a step closer to understanding the forces underlying the complex behavior of the Min system. Furthermore, it is likely they will give rise to new questions that will guide future studies in the ongoing search for a point of inhibition within the Min system, a potential target for development of new antimicrobial agents.

1.11 Technical Appendix to the Introduction

The work in this thesis primarily takes advantage of the information provided by CD spectroscopy, enzyme kinetics, and dissociation constant measurements to address our questions regarding conformational change and MinE function. Some background into the theory of these techniques is provided in the following sub-sections.

1.11.1 Circular Dichroism Spectroscopy

CD spectroscopy makes use of the ability of chiral molecules to differentially absorb left- and right-handed components of circularly polarized light. These differences are measured in elipticity (θ). In the case of proteins, this chirality is imposed by the three dimensional structure, with different secondary structure elements giving rise to different characteristic spectra in the 190-250 nm range (Fig. 1.10) (44, 45).

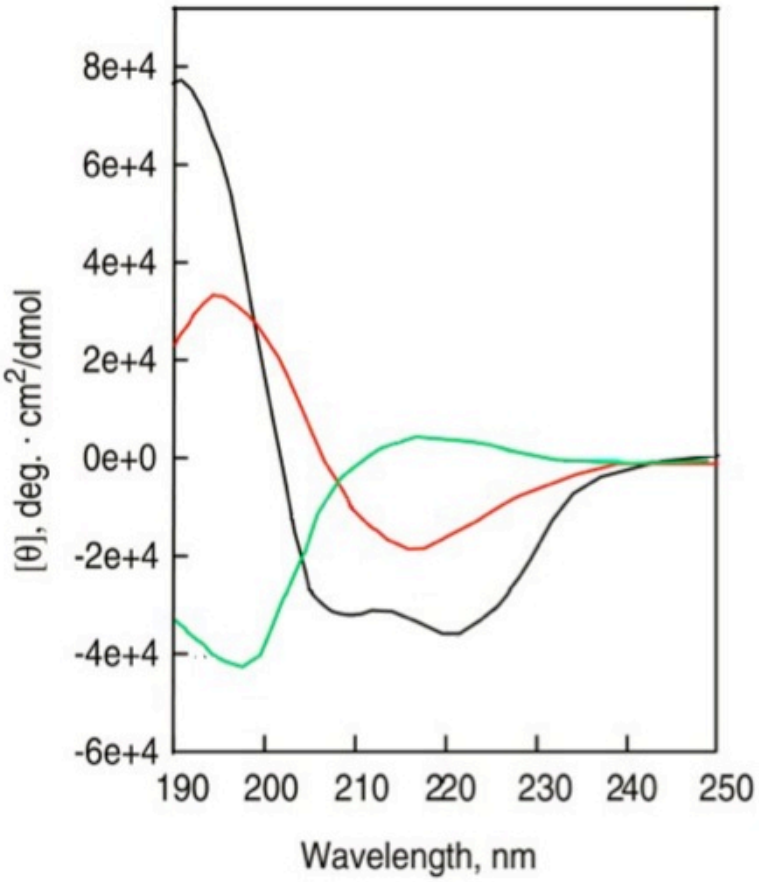

Figure 1.10: Characteristic CD spectra of secondary structure elements. α-Helix (black) produces a maximum at 193 nm and minima at 208 nm and 222 nm; β-sheet (red) gives a maximum at 196 nm and a minimum at 218 nm; and random coil spectra (green) have a minimum at 190 nm and a maximum at 212 nm. Figure adapted from Greenfield, 2007, Nature Protocols (appendix A2) (44).

The secondary structure content of a sample can be estimated from its CD spectrum using deconvolution algorithms such as those used in the software CDPro (46-49). These algorithms make use of spectral libraries of proteins of known secondary structure content to find a linear combination that best fits the data. The accuracy of a fit tends to increase with the number of proteins in the library and can also be improved by selecting libraries that include structurally similar proteins: soluble, membrane, or denatured. Collecting spectra in the lower wavelength range, (below 200 nm), can also improve the fit, however, the signal-to-noise ratio tends to be low in this range (45, 47). Furthermore, ions present in buffer solutions, particularly chloride, absorb below 200 nm, further decreasing the signal-to-noise ratio (45). For these reasons there can be a trade-off between spectrum accuracy and range, with the spectral range of 200 – 250 nm typically being the minimum required for deconvolution (47).

1.11.2 Applications of the Hill Equation

The Hill equation is commonly used to define ligand binding interactions, in particular those that involve cooperativity. In a cooperative system, binding events are dependent; the likelihood of a subsequent binding event is either increased or decreased due to a previous event (50). The classic example of this phenomenon is the positive co-operativity of the binding of oxygen to hemoglobin (51, 52). Each oxygen molecule bound increases the affinity of the adjacent binding sites for oxygen thereby making the next binding event more likely. These co-operative relationships are defined by the Hill equation:

$$\Theta = \frac{[L]^h}{[L]^h + (K_{0.5})^h}$$

Where Θ is the fraction of ligand bound, L is the concentration of free ligand, $K_{0.5}$ is the concentration at which half of the ligand is bound and h is the Hill coefficient, which is a measure of the co-operativity within the system (50).

In the case of the Min system the precise nature of the co-operativity has yet to be defined but it has an impact on two measurements made in this work: the binding of MinE to lipids and the kinetics of MinE-stimulated MinD-catalyzed ATP hydrolysis.

Binding parameters of the interaction between MinE and lipids can be determined by monitoring the MinE elipticity at 208 nm as a function of lipid concentration. In this case fraction bound was expressed as:

$$\Theta = \frac{\theta_{MRE,x}}{\theta_{MRE,Max}}$$

Where $\theta_{MRE, x}$ is the elipticity measured at lipid concentration x and $\theta_{MRE, Max}$ is the elipticity at saturation. By fitting experimentally determined fraction bound to this equation the dissociation constant and Hill coefficient of the MinE-lipid interaction were obtained.

The second application of the Hill equation used in this thesis was in the assessment of the kinetics of the interaction between MinD and MinE. The ATPase activity of MinD is stimulated 10-fold in the presence of MinE (28, 30, 31), which provides a useful tool for assessing the relative affinity of the interaction between the two proteins by measuring the activity of MinD as a function of MinE concentration. Assuming that ATP hydrolysis rates are proportional to the amount of MinD that is bound, the fraction of MinD bound to MinE is represented by:

$$\Theta = \frac{v_0}{V_{Max}}$$

where v_0 is the initial rate of MinE-stimulated ATP hydrolysis at a given MinE concentration, and V_{Max} is the maximum rate of ATP hydrolysis. This can then be related to the Hill equation, by considering MinE as the ligand. In this case, the $K_{0.5}$ is the concentration of MinE required to reach half maximum stimulation of MinD, and is an indirect measure of an apparent binding affinity for the MinE-MinD interaction.

Chapter 2: Materials and Methods

2.1 Peptides and Plasmids

The peptide MinE12-30 was synthesized by Genscript and amino acid analysis was carried out by Rey Interior at Sick Kids Hospital to determine the concentration of a stock solution made in sterile, nuclease free water. Pet30a (+) plasmids containing *min* genes from *N. gonorrhoeae* were obtained from Saud Ayed (MinD), Dr. Houman Ghasriani (MinE) and Chris Hart via Dr. Goto (MinE-I24D, hereafter referred to as I24D)(31). These plasmids contain a kanamycin resistance gene, and a C-terminal hexahistadine tag preceded by a non-native Leu-Glu sequence introduced by the cloning process.

2.2 Mutagenesis

All primers were synthesized by Integrated DNA Technologies. N-terminal truncation mutants of MinE and I24D missing the first 11 amino acids were created in a two-step process with the oligonucleotide sequences shown in Table 2.1. The first set of primers, were used on the MinE and I24D plasmids to create constructs missing the first five residues: MinE6-87 and I24D6-87. These constructs were used with the second set of mutagenic primers to produce MinE12-87 and I24D12-87.

Reaction mixtures were prepared based on Qiagen Quikchange Site-Directed Mutagenesis protocols containing 18.5 µL nuclease free double distilled water (ddH_2O), 0.75 µL dimethylsulphoxide (Biorad), 1 µL of each of the 10 mM forward and reverse

primer stocks, 1 µL of 10 mM nucleotide triphosphate mixture (dNTP, Stratagene), 0.5 µL of 10 ng/µL template, and 2 µL of 2.5 U/µL Pfu Turbo polymerase (Stratagene). Reaction tubes were placed in a Biorad MJ Mini 48-Well Personal Thermal Cycler running the program shown in Table 2.2.

PCR products were run on a 2% agarose gel containing 0.001 mg/mL ethidium bromide to determine the success of PCR reactions. Electrophoresis was carried out in 0.5 M TAE buffer (20 mM Tris, 10 mM Acetic acid, 0.6 mM EDTA) for 30 minutes at 100 V on a Fisherbrand Power Mini apparatus. Successful products, as determined by visualization under UV light, were cleaned up using Pellet Paint (Novagen) according to the manufacturer's protocols.

Plasmids were sequenced at the Genomics Innovation Center at the Ontario Health Research Institute. Results were aligned with the original and desired MinE nucleotide and protein sequences (4) using BLAST analysis on the National Center for Biological Innovation website (34, 35). Translation of the sequencing results is shown in the appendix (Table A1).

Table 2.1: Primer sequences used in successive mutagenesis reactions. Primers were used to create truncations containing residues 6-87 with the MinE and I24D plasmids and 12-87 with the MinE6-87 and I24D6-87 plasmids generated in the previous reactions.

Truncation	Primer Sequence
6-87	Forward: 5'GTTTAACTTTAAGAAGGAGATATACATATGTTATTCGGTAGAAAGCAG AAAACGGCAACCGTTGCCCG Reverse: 5'CGGGCAACGGTTGCCGTTTTCTGCTTTCTACCGAATAACATATGTATAT CTCCTTCTTAAAGTTAAAC
12-87	Forward: 5'GTT TAA CTT TAA GAA GGA GAT ATA CAT ATG CAG AAA ACG GCA ACC GTT GCC CGC GAC CGCC Reverse: 5'GGCG GTC GCG GGC AAC GGT TGC CGT TTT CTG CAT ATG TAT ATC TCC TTC TTA AAG TTA AAC

Table 2.2: Thermal cycle program used to produce truncations through mutagenesis on the MinE and I24D plasmids.

Step	Temperature (°C)	Time (min)
1	95	2
2	95	1
3	Gradient 55-65	1
4	68	6
5	Go to step 2 29 times	
6	72	10
7	4	hold

2.3 Transformation of DNA into Competent Cells

Plasmids were transformed into chemically competent DH5α or BL21 (DE3) cells (Invitrogen) for mutagenesis or protein expression respectively using established protocols (53). 10 ng/μL of plasmid DNA was introduced into a 20 μL cell aliquot and allowed to incubate on ice for 20 minutes. Cells were then heat-shocked for 2 min at 42°C followed by another 2 min on ice. Cells were diluted with 175 μL of Luria-Bertani

(LB) broth (54)(Lennox, Bioshop) and placed on a Barnstead lab-line MaxQ 4000 shaking incubator at 37°C for 1 hour. After incubation, cells were spread onto LB agar plates with 50 μM kanamycin and incubated for 16 hours at 37°C.

2.4 Plasmid Production and Purification

A well-delineated DH5α colony was selected from transformation plates and inoculated into 50 mL of LB media in a 250 mL Erlenmeyer flask with 50 μM of kanamycin (Bioshop). Cultures were shaken at 220 rpm and 37°C for 16 h. After incubation, cells were harvested by centrifugation in a BC Spinchron 15R centrifuge (Beckman Coulter) with a BC C6010 fixed angle rotor at 6000xg and 4°C for 15 min. Plasmids were purified from pellets using a Qiagen HiSpeed Midi Prep kit followed by a GenElute PCR cleanup kit (Sigma) using the manufacturer's protocols. Plasmids were stored at -20°C until required for protein expression or mutagenesis.

2.5 Bacterial Growth and Min Protein Expression

Min protein overexpression was carried out as previously described (41, 55). A well-delineated BL21 (DE3) colony was selected from plates and inoculated into 200 mL of LB media with 50 μM kanamycin in a 500 mL Erlenmeyer flask. This pre-culture flask was placed on a shaking incubator for 16 hours at 37°C and 220 rpm. The optical density at 600 nm (OD_{600}) of the pre-culture flask was determined after incubation using an Ultrospec 2100pro UV/Visible spectrophotometer. The volume of pre-culture

required to generate a starting OD_{600} of ~0.1 was transferred into a Fernbach flask containing 1 L of M9 media; 48 mM sodium phosphate, 22 mM potassium phosphate, 8.5 mM NaCl, 0.1 mM $MgSO_4$, 10 µM $CaCl_2$, 0.1% (w/v) ammonium chloride, 0.3% (w/v) D-glucose, 50 µg/mL kanamycin (all Bioshop) and 0.1% (v/v) MEM vitamins (Invitrogen) or LB broth (56). Culture flasks were shaken in a Barnstead lab-line MaxQ5000 shaking incubator at 220 rpm and 37°C for 3-4 hours and monitored until the OD_{600} was between 0.5 and 0.7. Isopropyl β-D-1-thiogalactopyranoside (Bioshop) was added to final concentration of 0.5 µM (56). Flasks were then shaken at 220 rpm at 16°C for 16 hours. Following incubation, cells were harvested by centrifugation at 3800xg for 10 minutes at 4°C in an Avanti JE (Beckman-Coulter) Centrifuge with a BC JA10.500 fixed angle rotor. Pellets were collected and stored at -20°C.

2.6 Min Protein Purification

MinD, MinE and MinE mutations and constructs were purified using nearly identical protocols as previously described (31, 41). A pellet from ~400 mL of bacterial culture was resuspended in 17 mL of lysis buffer (50 mM Tris-HCl, 250 mM NaCl, 10 mM Imidazole, pH 8.5, all Bioshop) with 15 mg of benzamidine (Bioshop). A protease inhibitor cocktail tablet (Roche) was also added for purifications of I24D and I24D12-87. Pellets were rocked on ice for 20 min then sonicated using a Fisher Scientific 500 Sonic Dismembrator with a titanium alloy microprobe (Fisher) three times at 45% amplitude, with a 1 second on, 1 second off cycle for 1 min. Resulting suspensions were centrifuged in a BC Avanti JE Centrifuge with a BC JA 25.5 fixed angle rotor at 16,000xg

for 20 minutes at 4°C. During centrifugation, 2.5 mL of HisPurNi-NTS resin (VWR) was equilibrated with 25 mL of lysis buffer. Supernatants were applied to equilibrated resin, incubated for 5 min, and then allowed to drain from the column. The flow-through was collected and reapplied to the column twice. The resin was then washed with two 25 mL aliquots of lysis buffer, followed by two 25 mL aliquots of wash buffer (50 mM Tris, 250 mM NaCl, 20 mM imidazole, pH 8.5). The protein was eluted by four 5 mL aliquots of elution buffer (50 mM Tris, 250 mM NaCl, 500 mM imidazole, pH 8.5). EDTA (Bioshop) was added to each eluate fraction to a concentration of 1.7 μM.

Protein samples were further purified by size exclusion chromatography using an SP75 Superdex 10/300 GL column with an AKTA FPLC apparatus. Size exclusion chromatography was done either immediately after nickel affinity chromatography, or after overnight storage at 4°C, with the exception of I24D and I24D12-87, which were always purified immediately after elution. Prior to FPLC injection, eluates were concentrated using Amicon Ultra 15 centrifugal concentrating units with a 10 kDa molecular weight cutoff for MinE and its mutants, and 30 kDa molecular weight cutoff for MinD. Centrifuge units were equilibrated with 10 mL of lysis buffer and centrifuged in a BC Spinchron 15R centrifuge with a BC S4180 swinging bucket rotor at 3800xg for 5 min at 4°C. After equilibration, 10 mL of eluate was added to the unit and centrifuged under the same conditions. Flow-through was discarded and the retained volume was mixed by pipetting, followed by addition of eluate back up to a 10 mL volume before another round of centrifugation. This was repeated until all 20 mL of eluate had been added to the unit and concentrated to a final volume of ~2 mL, or 4 mL in the case of WT MinE. 2 mL of concentrated sample was injected onto the size exclusion column,

which had been pre-equilibrated with size exclusion buffer (50 mM Tris-HCl, 100 mM NaCl, 0.2 mM EDTA, pH 8.5) and run at a flow rate of 0.5 mL/min. Progress was monitored via UV absorbance at 280 nm. MinD and MinE eluted at ~12 mL in a single peak that was collected over a 1.5 – 2 mL volume in 0.5 mL fractions. Fractions were pooled and stored at 4°C for use in characterization studies.

2.7 SDS-PAGE

Purity of protein samples was assessed using sodium dodecyl sulfate polyacrylamide gel electrophoresis (SDS-PAGE). 15 well 4-20% precast gradient gels (Thermo Scientific) were loaded with 13-15 μL of sample in 1X loading buffer (5% (w/v) SDS, 10% (v/v) glycerol, 0.005% (w/v) bromophenol blue, 62.5 mM Tris-HCl pH 6.8). 2 μL of pre-stained EZ-Run protein markers (Fisher) were run alongside the samples. Gels were run in a Bio-Rad SDS-PAGE apparatus for 35 min at 150 V in Tris-HEPES-SDS running buffer (0.1 M Tris-HCl, 0.1 M HEPES, 0.035 M SDS). Gels were stained overnight with Coomassie blue (50% methanol, 10% acetic acid, and 0.1% Coomassie brilliant blue) and destained using 10% acetic acid, 40% methanol solution.

2.8 Mass Spectrometry

The size of purified Min proteins was confirmed using a Bruker Microflex LT matrix assisted laser desorption ionization (MALDI) mass spectrometer. The matrix was prepared by saturating a 75% acetonitrile, 0.01% Trifluoroacetic acid solution

with sinopinic acid (all Sigma). The resulting suspension was centrifuged for 30 seconds at 16,0000xg. 5 µL of supernatant was mixed with 5 µL of Min protein sample or lysozyme standard and deposited in 1 µL aliquots on a MSP 96 polished steel target (Bruker). After samples had dried, the plate was inserted into the spectrometer and samples were excited at 80-90% laser power with an offset of 18%, a range of 30%, and at a frequency of 60 Hz. Spectra were collected for mass to charge ratios (m/z) in the range of 2150 m/z to 22500 m/z. Lysozyme standards were applied to MinE spectra by calibrating with both the single and doubly charged peak of lysozyme and applying that calibration to the MinE spectra post collection.

2.9 Protein Concentration Determination

Concentrations of purified Min proteins were determined through standard bicinchoninic acid assay (BCA) using a bovine serum albumin standard curve (both Thermo). (57, 58)

2.10 Preparation of Lipid Vesicles

Large unilamellar vesicles (LUVs) were prepared from chloroform stocks of 10 mg/mL 1,2-dioleoyl-*sn*-glycero-3-[phosphor-*rac*-(1-glycerol)] (DOPG, Avanti), or 25 mg/mL *E. coli* total lipid extracts (57.5% Phosphatidylethanolamine, 15.1%Phosphatyidylglycerol, 9.8% cardiolipin)(Avanti). Chloroform stocks were placed in a glass test tube and solvent evaporated under a stream of argon over 30 minutes. The resulting film was stored in the fume hood for 12 hours to ensure complete solvent

removal. The lipid film was resuspended to a concentration of 10 mg/mL lipid in either 10 mM Tris-HCl, pH 8.5 for circular dichroism experiments or 25 mM Tris-HCl, 50 mM NaCl, pH 8.0 for kinetic studies. Before use, lipids were extruded using Hamilton syringes in an Avanti Mini-Extruder. DOPG was extruded using a 0.1 μm filter at room temperature. *E. coli* lipids were extruded first with a 1 μm filter, and then through a 0.1 μm filter at ~50°C.

2.11 Circular Dichroism Spectroscopy

The secondary structure of MinE and the effect of lipids on that structure was assessed using CD. Prior to CD, MinE was transferred from size exclusion buffer into 10 mM Tris at pH 8.5. Buffer exchange was carried out using either dialysis or a centrifugal filter unit. Dialysis was carried out for ~3 mL of MinE in 6,000-8,000 Da molecular weight cut off dialysis tubing against a total of 4 L of 10 mM Tris over a 24 hour period with 3 buffer changes. In some instances buffer exchange was done with a centrifugal filter unit instead of dialysis. Briefly, ~3 mL of purified MinE was diluted with 10 mL of 10 mM Tris and spun for 5 min at 3800xg in a Spinchron 15R centrifuge with a S4180 swinging bucket rotor. The retained solution volume was mixed by pipetting, and then the volume brought back up to 10 mL by addition of 10 mM Tris pH 8.5, and spun for 2 min at the same speed. This was repeated until a total of 40 mL had been added to the initial MinE. When approximately 6 mL remained, spin times were reduced to 1 min, and the sample was mixed between spins until concentrated back to its initial volume of 3 mL. Buffer exchanged samples were centrifuged for 1 minute at 16,000xg in an Eppendorf 5415D tabletop centrifuge to sediment any aggregates. This stock was used

to make 425 µL samples of ~15 µM MinE in 10 mM Tris pH 8.5 for CD spectroscopy. NaCl was added to 130 µM or 40 µM where solubility was a concern.

Samples were placed in a 0.1 cm quartz CD cell (Hellma), which had been cleaned by overnight treatment with nitric acid followed by a 30-minute rinse in distilled water. The cell was then rinsed for 1 minute with ddH_2O followed by 70% ethanol, then dried under an argon stream. Spectra were collected on a JASCO J-810 or J-815 spectropolarimeter. Spectra were collected at room temperature from 200 to 250 nm over 8 accumulations with a 0.5 nm pitch at 0.2 nm/min, a response time of 8 s and a bandwidth of 1 nm.

Spectra were converted to mean residue ellipticity (θ_{MRE}) using:

$$\theta_{MRE} = \frac{\theta}{NCl}$$

where θ is the ellipticity in millidegrees, N is the number of peptide bonds in the protein, C is the concentration of protein in dmol/cm^3 and l is the path length in centimeters (44).

2.12 MinE Lipid-Binding Affinity Measurements

To assess the affinity of MinE for binding to LUVs comprised of either DOPG or *E. coli* total lipid extracts, samples were prepared for CD with various concentrations of LUVs while maintaining a constant concentration of MinE (~15 µM). Protein

concentrations for each sample were verified by a BCA assay and the average was used in calculations of θ_{MRE} and protein-lipid dissociation constants. Lipid concentrations were varied from 0 to 0.7 mg/mL for studies done with DOPG and from 0 to 2.0 mg/mL for those done with *E. coli* total lipid extracts. Due to the decrease in signal intensity at high concentrations of both salt and lipid NaCl was excluded from titration samples in order to access a wider range of LUV concentrations. Blanks of alternating concentration points were prepared and applied to spectra after collection.

The difference in molar ellipiticity at 208 nm between the spectrum of MinE without lipids and that in the presence of x mM lipid ($\Delta\theta_{MRE,\,x}$) was calculated for each spectrum. The fraction of MinE bound to lipid at each concentration was determined from the ratio of $\Delta\theta_{MRE,\,x}$ to the maximum difference observed under saturating conditions ($\Delta\theta_{MRE,\,Max}$). These values could then be used to find the dissociation constant (K_d) using the Hill equation:

$$\frac{\Delta\theta_{MRE,x}}{\Delta\theta_{MRE,Max}} = \frac{[L]^h}{[L]^h + (K_d)^h}$$

where L is the concentration of lipid and h is the Hill coefficient.

The interaction between MinE and lipids was assessed for reversibility by diluting a titration sample post read, incubating for 5 minutes, and then reading again. The fraction bound was calculated and compared to the theoretical fraction bound calculated with the binding parameters determined by that particular titration. This procedure was carried out in duplicate. The interaction with both DOPG and *E. coli* total

lipids was reversible with an average difference of 12% between the expected and measured fraction bound.

2.13 Secondary Structure Determination

The secondary structure content of MinE and its mutants was analyzed using CDPro (46-49) in conjunction with JASCO's spectral analysis software. Structure percentages were calculated by fitting the measured spectra to two reference protein sets SP37A and SP43, which contain 37 and 43 soluble proteins respectively (47). The calculations were carried out using fitting programs: SELCON3, CONTIN, and CDSSTR (46-49). Outputs from the three programs were averaged to determine the percent helix, sheet and undefined contributions to the structure. Standard deviation was calculated for the average output to reflect the agreement of the fits between fitting algorithms and protein libraries.

2.14 ATPase Assay

The apparent affinity of the interaction between MinE and MinD was determined by monitoring the MinE-stimulated rates of MinD-catalyzed hydrolysis of ATP (31). ATP hydrolysis reactions were monitored in the malachite green colorimetric assay, which determines the concentration of free phosphate in solution (59-61). Reaction mixtures at pH 8.2 contained 2.7 μM MinD, 0.5 mg/mL DOPG LUVs, 65 mM Tris, 80 mM NaCl, 5 mM $MgCl_2$, 50 mM KCl, 1 mM ATP and varying concentrations of MinE. 35 μL aliquots were taken at 5, 15, 24, 33, and 41 minutes and were boiled for 1

minute in a water bath to denature the enzyme and stop the reaction. These reaction mixtures were centrifuged for 4-5 min to sediment the LUVs. 15 μL of supernatant was added to a 96 well plate preloaded with 70 μL of malachite green reagent (0.35 mM malachite green, 9 mM Ammonium molybdate, 0.15% (v/v) Tween-20 that was added immediately before use). The plate was incubated for 15 minutes at room temperature before being read using a Molecular Devices SpectraMax Plus 96 well plate reader at 620 nm. A graph of absorbance versus time was generated, giving rise to a linear trend that was fit to an equation of a straight line. The initial rate of the reaction was determined from the slope of this line. Absorbance readings were converted to phosphate concentrations using a standard phosphate curve.

Reaction rates were plotted as a function of MinE concentrations and fit to the Hill equation to obtain kinetic parameters governing the reaction. In this case the ratio of the measured rate to the maximum rate of ATP hydrolysis was assumed to provide a measure of the fraction of occupied MinE binding sites as previously described (31).

Chapter 3: Results

3.1 Generation of Truncations

Membrane association of MinE had previously been attributed to its interaction with MinD, which is found at the bacterial inner membrane surface in fluorescence microscopy experiments with labeled MinD (14). However, recent reports have demonstrated that MinE has the ability to independently associate with the membrane via its N terminal MTS (32, 33). A construct of MinE was created, which lacks the N-terminal MTS, in order to study this membrane association and its role in the stimulation of the ATPase activity of MinD. In addition, removal of the MTS in the I24D mutant was carried out to determine the possible role of this sequence in the conformational transition between the 6-stranded and the 4-stranded MinE dimer. This mutant is expected to have the 4-stranded conformation similar to that observed in the MinE-I24N complex with MinD since Ile-24 is buried in the hydrophobic core of the 6-stranded structure of MinE (31, 33).

Truncations were produced by site directed mutagenesis in two steps, the first removing residues 2-5, and the second 6-11. As shown in Figure 3.1, for the first set of mutagenesis reactions, PCR products for both plasmids could be detected at all annealing temperatures at the expected molecular weight, between the 5 and 6 kbp markers on the ladder. These products gave rise to successful transformants, which were used to isolate plasmid DNA for sequencing. As shown in the appendix (Table A1), mutagenesis reactions yielded the expected truncations, which were used in subsequent studies described below.

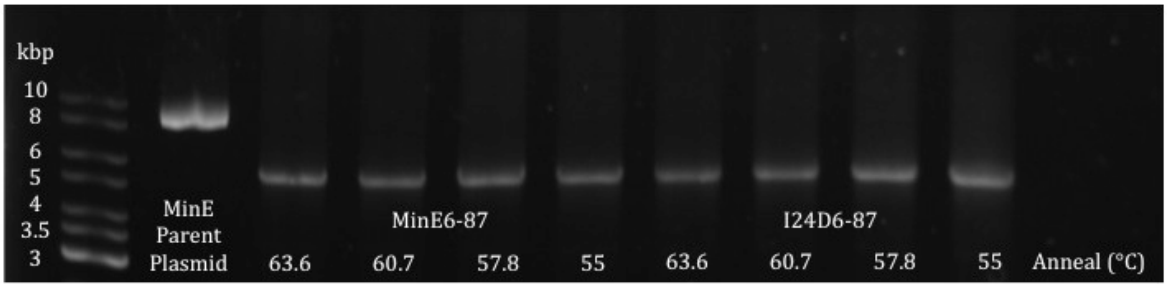

Figure 3.1: Agarose electrophoresis gel of PCR products from site-directed mutagenesis reactions of MinE with primers shown in Table 2.1. PCR reactions were carried out using MinE and I24D plasmids at the annealing temperature indicated under each lane. A sample of the MinE parent plasmid used in the mutagenesis reactions is also shown.

3.2 Expression and Purification of Min Proteins

Min protein expression and purification was monitored using Coomassie-stained SDS-PAGE, examples of which are shown in Figure 3.2A and B for MinE and MinD respectively. An increase in intensity at the expected molecular weight, 11 kDa for MinE and 37 kDa for MinD, can be observed from the pre-induction sample (lane 1) to the post induction sample (lane 2), indicating successful expression as previously described (41, 55).

Min proteins were purified from cell pellets by successive nickel affinity and size exclusion chromatography steps, which have also been previously described (31, 41). Coomassie-stained gels of representative examples of purifications are shown in Figure 3.2A and C for MinE and MinD, respectively. A high intensity band is observed in the whole cell lysate (lane a) and soluble fraction of the lysate (lane b) that is absent in the flow-through from the nickel affinity column (lane c). Wash steps with increasing concentrations of imidazole, were also devoid of Min protein (lanes d and e) while the high concentration of imidazole eluted both Min proteins in >90% purity (lane f).

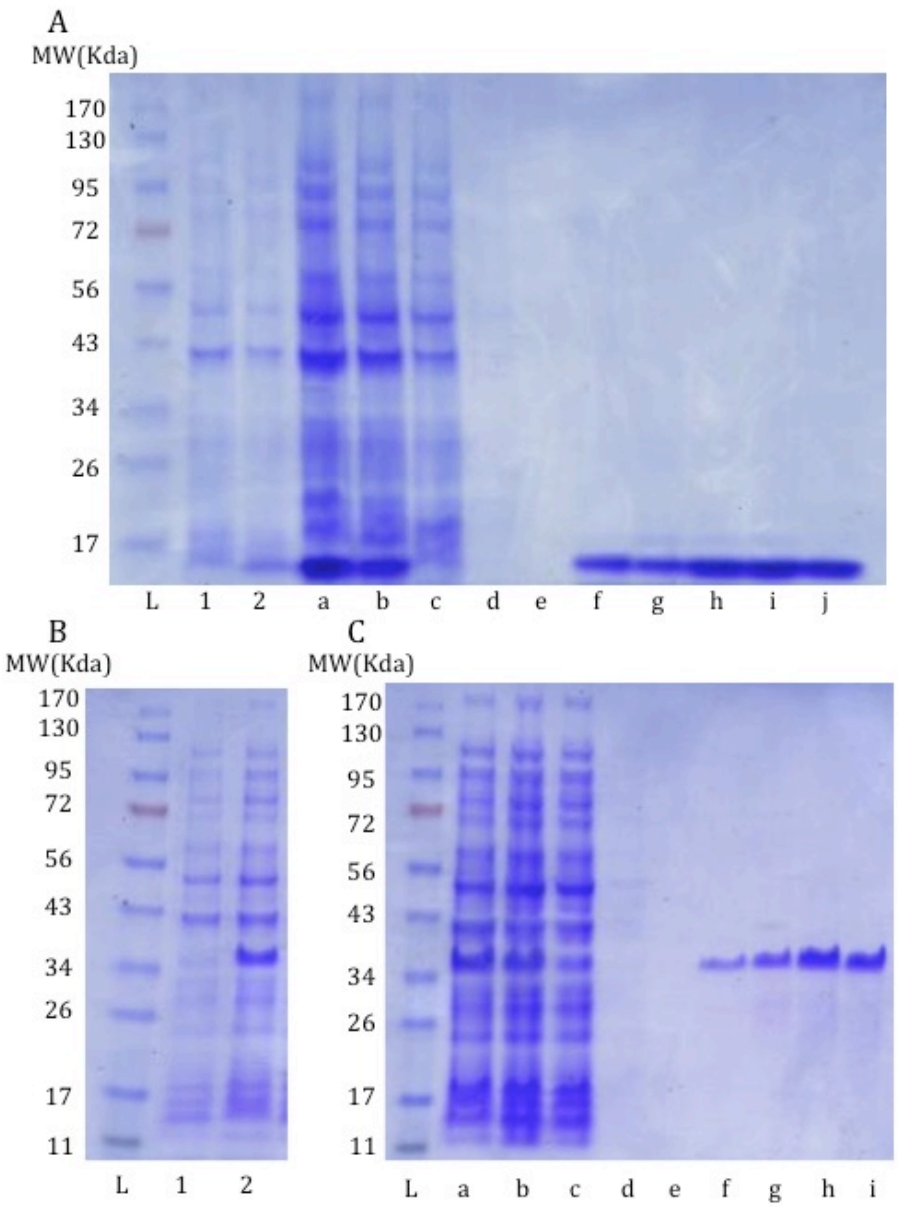

Figure 3.2: Coomassie-stained SDS-PAGE analysis of Min protein expression and purification. A) Expression and purification of MinE. B) MinD expression samples C) MinD purification samples. In all cases the ladder is denoted as L. Samples pre and post induction with IPTG are shown in Lanes 1 and 2 respectively. Samples taken during the purification steps are shown in lanes a-j, specifically; a) whole cell lysate; b) soluble fraction; c) nickel column flow-through; d) wash with 10 mM imidazole; e) wash with 20 mM imidazole; f) elution with 500 mM imidazole; g-j) fractions taken from main elution peak in size-exclusion chromatography.

Min proteins were then applied to a Superdex SP75 FPLC size exclusion column for a final purification step. Elution was monitored by absorbance at 280 nm, and found to give rise to a profile with Min proteins eluting in a peak over a 1.5-2 mL volume at ~12-12.5 mL as previously observed (31, 41). As shown in Figure 3.2C the purity of FPLC-purified samples was typically on the order of >95%. In some cases, MinD was observed to elute as a broad or asymmetrical major peak (Fig. 3.3, purple trace). In those cases the eluate was reapplied to the same column (Fig. 3.3, green trace) to improve the purity of the sample.

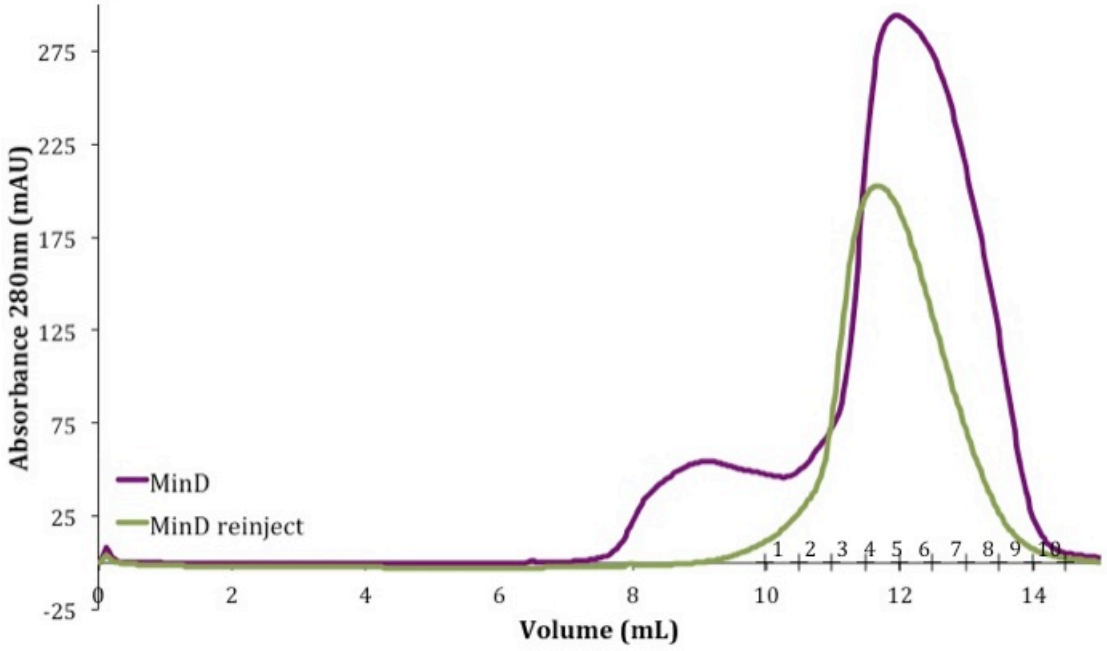

Figure 3.3: Example of size exclusion chromatography profile for MinD. ~2 mL of nickel affinity chromatography-purified MinD was applied to a Superdex SP75, which had been equilibrated in 50 mM Tris-HCl, 100 mM NaCl, and 0.2 mM EDTA at pH 8.5. Elution was monitored by absorbance at 280 nm (purple), and fractions 3-6 (indicated on the x-axis) were pooled and re-injected onto the column (light green).

Size exclusion chromatography purification of MinE gave rise to a major peak at ~11 – 12 mL, with an additional peak eluting at the void volume, in line with previous observations (31, 41). MinE was primarily found in the 12 mL peak, giving rise to >95% pure protein as shown in Figure 3.2A. A small difference in elution profiles was observed for the I24D mutant (Fig. 3.4A, dark green), with elution occurring ~0.5 mL earlier than the WT protein. A similar difference was also observed in the size exclusion chromatography profiles of WT versus I24D truncation mutants (Fig. 3.4B).

One difference noted during the purification of both MinE truncation mutants is that they could be purified to greater than 10-fold higher concentrations than what was observed for full-length samples. This indicates that the membrane targeting sequence may be responsible for the relatively poor solubility of full-length MinE.

3.3 MALDI Mass Spectrometry

MALDI mass spectrometry was used to confirm the identity of each sample. As shown in Figure 3.5, all samples gave a high intensity peak at the expected m/z for both the single and doubly charged species.

Average molecular weights for each construct were calculated using the m/z of both the single and doubly charged species of three independent preparations (Table 3.1).

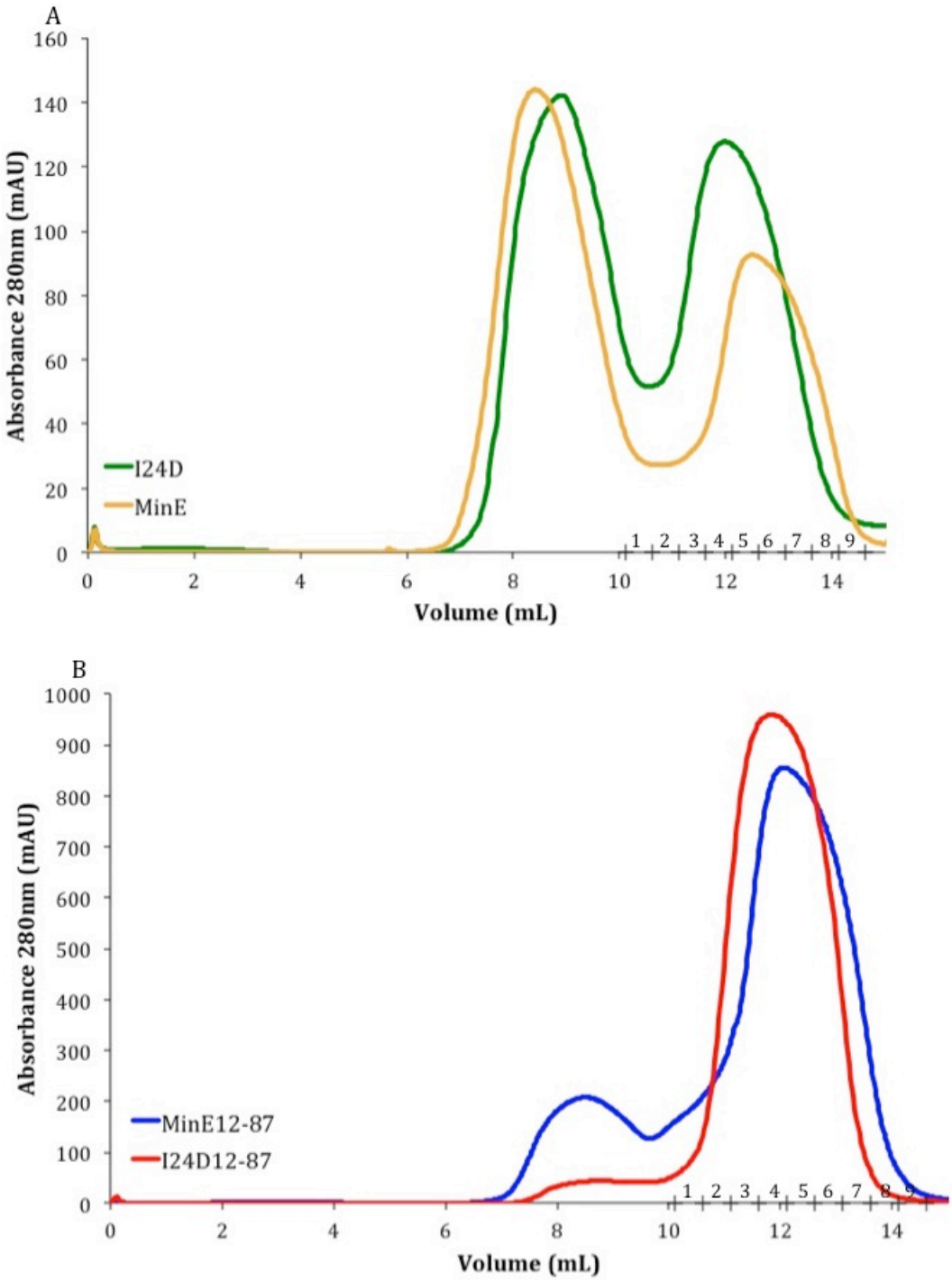

Figure 3.4: Examples of size exclusion chromatography profiles for WT and mutant MinE. Nickel-affinity purified samples were applied to the Superdex SP75 column equilibrated in 50 mM Tris-HCl, 100 mM NaCl, and 0.2 mM EDTA at pH 8.5, and elution was monitored by absorbance at 280 nm. Profiles are shown for; A) MinE (yellow) and I24D (dark green); and B) MinE12-87 (blue) and I24D12-87 (red). Fractions collected are marked on the x-axis.

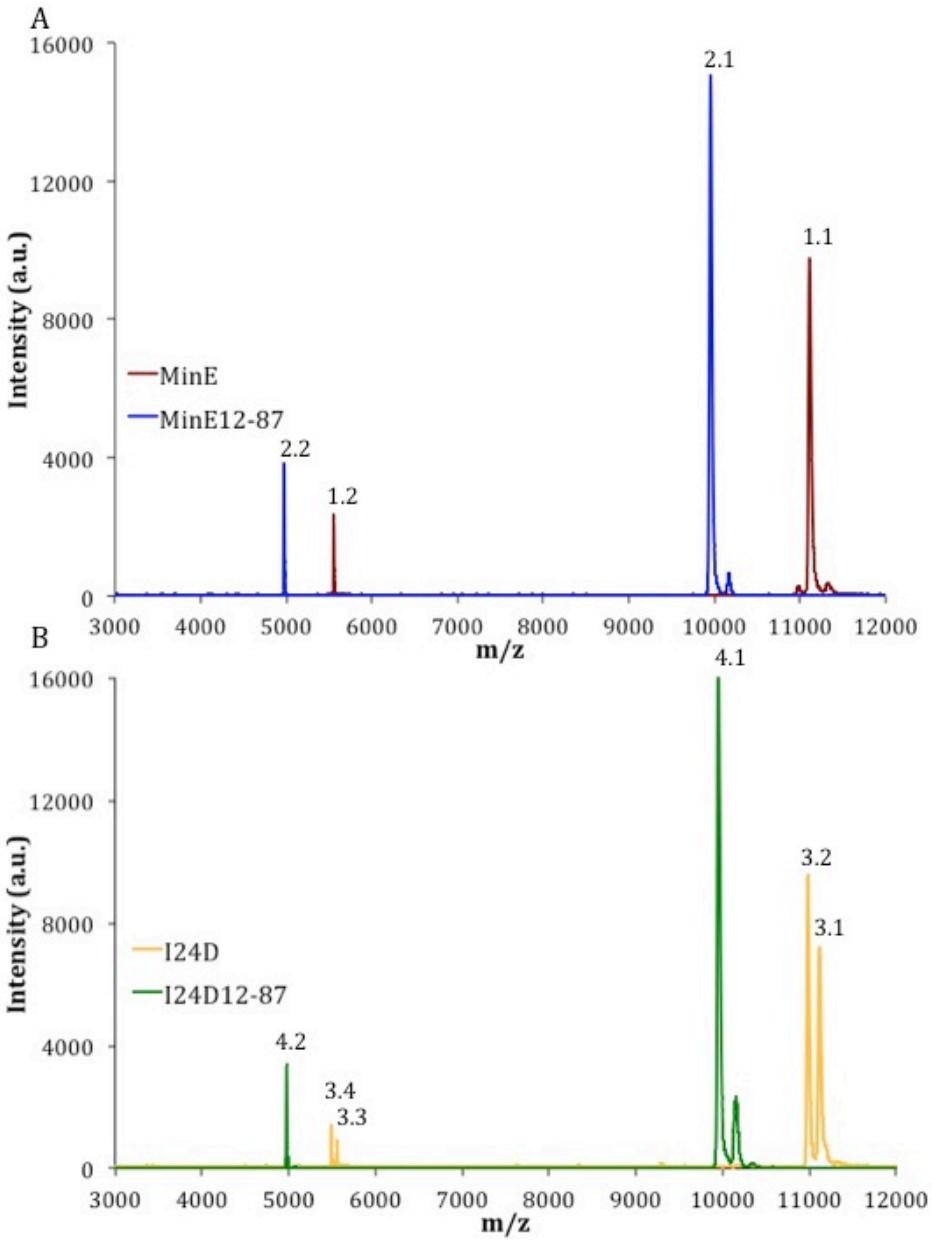

Figure 3.5: Representative MALDI mass spectra for purified MinE and its mutants. Samples were deposited on a Bruker polished steel target and excited at 80-90% laser power. A) MinE (red) with peaks at m/z 11111.2 (1.1) and 5555.2 (1.2) representing the single and doubly charged states. MinE12-87 (blue) has peaks at m/z 9955.2 (2.1) and 4974.2 (2.2). B) I24D (yellow) shows a double peak for both the single and doubly charged species. The difference in these peaks corresponds to a loss of the N terminal methionine (I24D-M1) with the single charged peaks at m/z of 11114.6 (3.1) and 10983.4 (3.2) for I24D and I24D-M1 respectively. The doubly charged peaks, (3.3 and 3.4) were found at m/z 5557.1 and 5491.6 for I24D and I24D-M1, respectively. I24D12-87 (green) had peaks at m/z of 9951.4 (4.1) and 4975.6 (4.2) representing the single and doubly charged species.

Table 3.1: Molecular weight of MinE samples as determined by MALDI mass spectrometry. Measured molecular weights were calculated using the m/z of both the single and doubly charged species for three independent samples and are reported plus or minus the standard deviation.

	Expected MW	Measured MW (Da)
MinE	11105.7	11110±10
I24D	11107.7	11120±20
I24D-M1	10976.5	10971±6
MinE12-87	9948.3	9955±6
I24D12-87	9950.3	9947±3

In all cases the measured molecular weight corresponded to expected values calculated based on the amino acid sequence. All species were intact, with the exception of I24D, which had a significant population with a molecular weight corresponding to the expected species missing the N-terminal methionine (I24D-M1). M1 has not been implicated in either membrane binding or MinD stimulation (31-33, 38) so no attempt was made to separate I24D-M1 from I24D. However, it was necessary to carry out the purification of I24D and I24D12-87 in the presence of additional protease inhibitors during cell lysis. This protease inhibitor cocktail was also added to the final purified samples, to prevent proteolysis.

3.4 Lipid Induced Conformational Change in MinE

As described in the Introduction, accumulating evidence suggests that MinE can bind to lipid membranes independent of any association with MinD (32, 33, 62). In order to determine the effect this association has on the structure of MinE, CD spectroscopy was performed on MinE in the presence and absence of LUVs comprised of DOPG (Fig. 3.6).

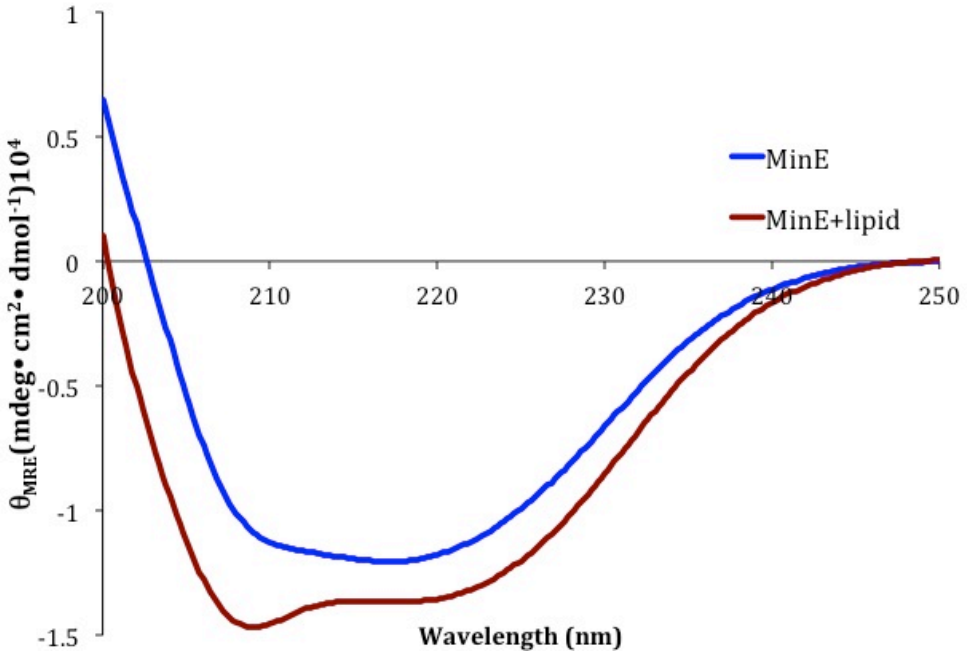

Figure 3.6: CD spectra of MinE in the presence and absence of LUVs. Samples contained ~15 μM MinE, 10 mM Tris-HCl at pH 8.5 either with (red) or without (blue) 0.7 mM DOPG.

As shown in Figure 3.6, in the absence of lipid the CD spectrum has a minimum that extends from ~208 nm to 220 nm, exactly as has been previously reported (41, 43). When this same experiment was repeated in the presence of LUVs comprised of the negatively charged synthetic lipid, DOPG, there was a decrease in ellipticity at 208 nm, indicating a significant change in secondary structure content. A similar spectral change was also observed if this experiment was performed with vesicles comprised of total *E. coli* lipid extracts.

Since the change in ellipiticity at 208 nm reflected the fraction of MinE bound to the vesicles, spectra were recorded at a range of lipid concentrations to determine the dissociation constant for the MinE-membrane interaction. An example of a titration series is shown in Figure 3.7A.

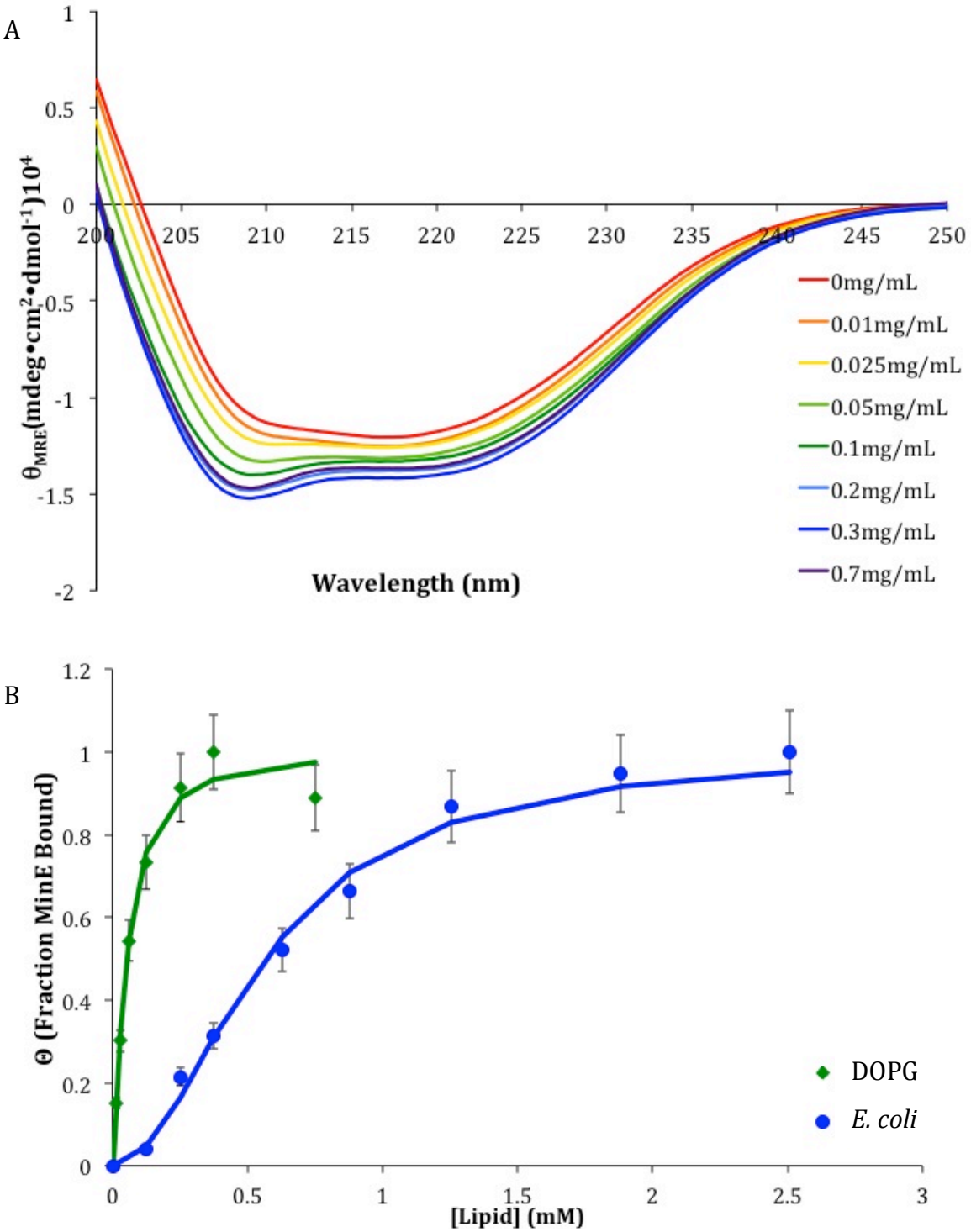

Figure 3.7: MinE lipid-binding affinity measurements by CD. A) Representative series of CD spectra obtained for~15 μM MinE, 10 mM Tris-HCl over a range of DOPG LUV concentrations. B) Fraction of MinE bound to LUVs comprised of DOPG (green) or *E. coli* lipid extracts (blue) over a range of lipid concentrations. Lines represent the best fit of the Hill equation to the data. Error bars represent the average percent relative standard deviation between triplicate experiments of fraction bound at each lipid concentration.

The fraction of MinE bound, calculated as the ratio of the molar elipticity at 208 nm versus that observed at saturation, was calculated at each lipid concentration and the series fit to the Hill equation (Fig. 3.7B). As summarized in Table 3.2, MinE had an approximately 10 fold greater affinity for binding vesicles made with the anionic lipid DOPG versus those made with *E. coli* lipids. Both binding curves were fit with a Hill coefficient that was greater than one, which indicates MinE is binding to the membrane with some cooperativity.

Table 3.2: Hill equation parameters for MinE-lipid interaction.

Lipid	K_d (μM)	h
DOPG	60±10	1.4±0.1
E. coli total lipid extract	560±80	1.7±0.3

3.5 Membrane Interaction of MinE Constructs

To determine if the conformational change observed upon MinE binding to lipids was similar to the conformational transition proposed to occur for MinD binding, CD spectra were acquired for I24D, which is expected to have a 4-stranded structure similar to that observed in the MinDE complex structure. As shown in Figure 3.8B, the CD spectrum of I24D is significantly different in shape from that of the WT spectrum (Fig 3.8A), consistent with the expected change in secondary structure content. The I24D spectrum also shows an additional change upon introduction of DOPG vesicles suggesting that this mutant is also capable of binding lipids, and that this is accompanied by a conformational transition. It should be noted that, unlike the spectra shown above, these were acquired in the presence of 130 mM NaCl to mimic the conditions used in MinD ATPase assays, although in the case of I24D a lower

concentration had to be used (40 mM) due to solubility considerations. WT spectra were also recorded in the presence of 130 mM NaCl to ensure membrane interaction was maintained under high salt conditions (Fig. 3.8A).

CD spectra of truncation mutants MinE12-87 and I24D12-87 were acquired in the presence and absence of lipid to confirm that lipid binding by MinE is mediated by the MTS (Fig. 3.9A and B). In the absence of lipid the shapes of spectra from both samples resembled the lipid-free spectrum of the corresponding full-length construct. Spectra did not show significant changes upon introduction of lipid, indicating neither mutant can undergo the membrane-induced conformational change observed with WT MinE. The absence of this conformational change with the truncation mutants is consistant with the removal of the MTS causing a loss of binding activity. Therefore the MTS appears to be responsible for mediating the interaction with lipids, along with the corresponding conformational change.

Since we were also interested in studying the functional characteristics of the minimal MinD-binding motif (MinE residues 12-30), we also wanted to confirm an absence of lipid-binding interaction for this peptide. As shown in Figure 3.9C, ellipiticity values were generally consistent with the absence of any strong structural propensity for this peptide. No signficant change was observed upon addition of DOPG vesicles, confirming that this peptide does not bind to lipid membranes under these conditions.

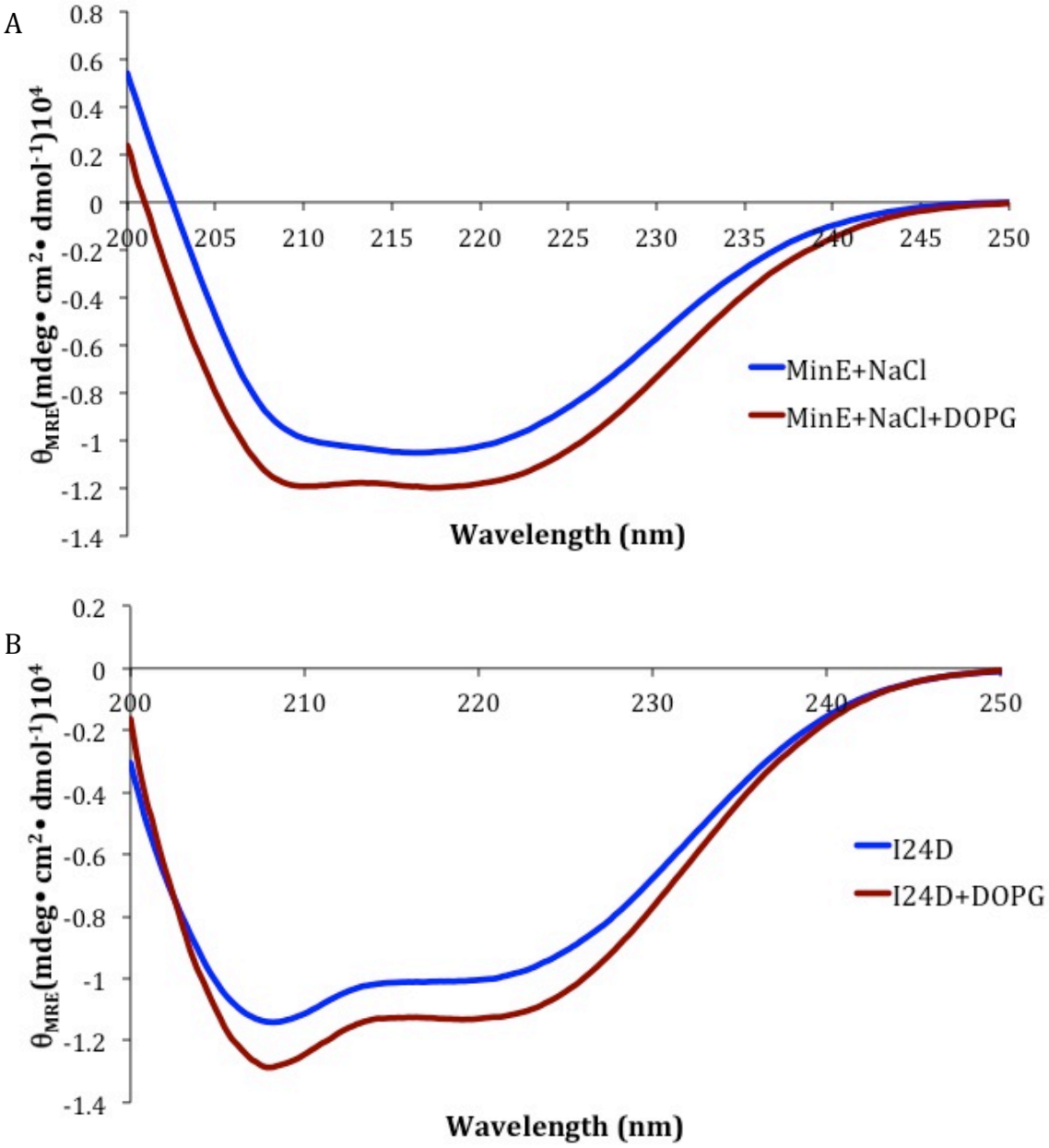

Figure 3.8: CD spectra of MinE and I24D with NaCl in the absence and presence of lipids. Spectra were collected containing ~15 μM I24D samples with either no DOPG (blue) or 0.5 mg/mL DOPG, (red) in 10 mM Tris-HCl, and 40 mM NaCl for I24D or 130 mM NaCl for MinE at pH 8.5.

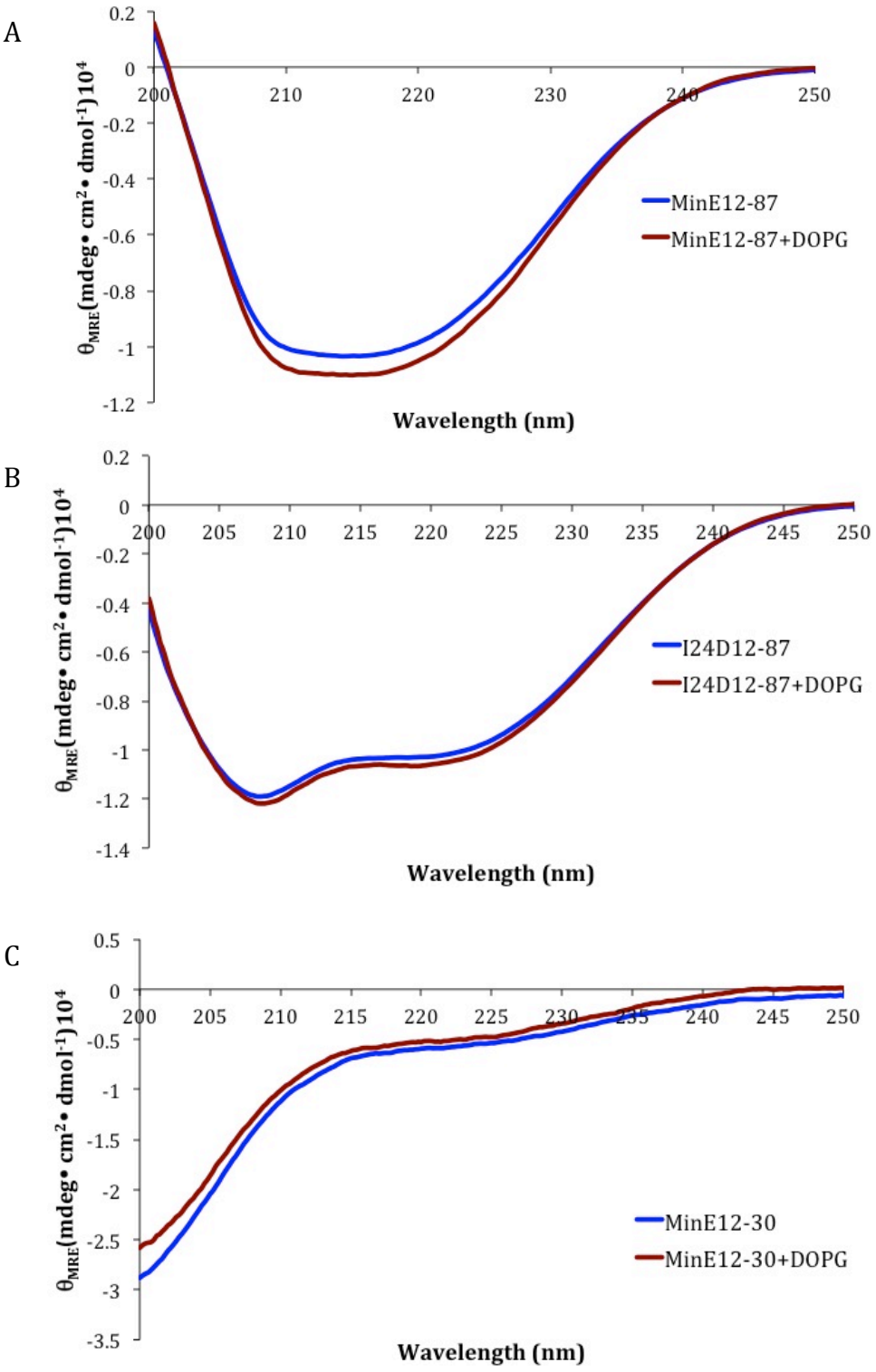

Figure 3.9: CD spectra of MinE MTS-truncation mutants in the absence (blue) or presence (red) of DOPG. A) MinE12-87 B) I24D12-87 C) MinE12-30. Samples contained ~15 μM protein or peptide, 0 or 0.5 mg/mL DOPG, 10 mM Tris-HCl, and 130 mM NaCl at pH 8.5.

3.6 Secondary Structure Deconvolution from CD Data

In order to extract secondary structure contributions from CD spectra, each curve was fit in CDPro using two libraries and three widely used fitting algorithms as described in Chapter 2.13 (Table 3.3)(46-49).

Table 3.3: Percent secondary structure composition of MinE and its constructs as determined by CDPro. Values are reported plus or minus the standard deviation of the average output from the three fitting algorithms each used with two protein libraries.

	Lipid	[NaCl]	Helix(%)	Sheet (%)	Turn (%)	Unordered(%)	n*
MinE	None	0	29±2	20±2	16±4	35±6	6
	DOPG		36±3	14±2	16±4	34±6	3
	E. coli		35±2	15±2	16±4	34±6	3
	None	130	28±1	21±2	16±4	35±6	2
	DOPG		32±2	17±2	16±3	35±6	2
I24D	None	40	29.5±0.7	17±4	18±4	36±7	2
	DOPG		36±2	13±2	17±4	34±6	2
MinE12-87	None	130	23.0±0.8	22±4	18±4	38±8	2
	DOPG		27±4	20±4	16±4	37±7	2
I24D12-87	None	130	33±2	14±3	18±4	36±6	3
	DOPG		33±1	14±3	18±4	36±6	3
MinE12-30	None	130	12±4	19±8	21±6	48±12	2
	DOPG		12±5	22±9	20±5	46±11	2

* Number of independent samples used in the analysis.

A t-test was carried out to identify statistically significant differences in secondary structure content caused by the addition of lipids. A table of the resulting p values is shown in the appendix (Table A2). Those samples that gave rise to lipid-dependent changes only showed differences in helix and beta structure content. As summarized in Figure 3.10, this was observed for both WT and I24D MinE, with lipid binding causing an increase in helix content and decrease in sheet content. As expected, MinE12-87, I24D12-87 and MinE12-30, all of which lack the N-terminal MTS, showed no significant structural change upon introduction of DOPG with confidence interval $p>0.005$. However, with a confidence interval of $p>0.01$ there is a statistically

significant increase in the helix content of MinE12-87 in the presence of lipid, which may indicate some residual lipid interaction.

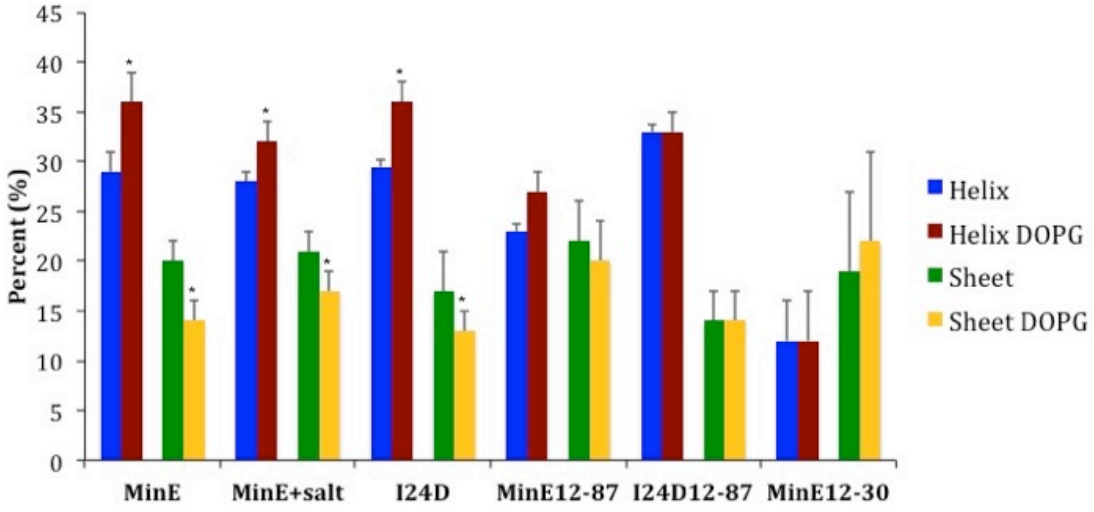

Figure 3.10: Secondary structure changes upon lipid binding. Percent α-helix (blue, red) and β-sheet (green, yellow) as predicted by CDPro analysis of CD spectra of MinE samples in presence (red, yellow) and absence (blue, green) of DOPG vesicles. Stars denote samples showing a statistically significant difference between predicted helix or sheet in the absence and presence of lipid ($p>0.005$).

3.7 Effect of the MinE-Membrane Interaction on MinD Stimulation

Having established that removal of the MTS prevents interactions between MinE and the membrane, we set out to test the effect of this change on the ability of MinE to stimulate the ATPase activity of MinD. This was monitored by an *in vitro* measurement of ATP hydrolysis rates using a malachite green-based assay for the detection of phosphate as previously described (31, 60). To confirm that the ATPase activity detected in the assay arose from MinE-stimulation of MinD-catalyzed ATP hydrolysis, a reaction was run with MinD, MinE, ATP, phospholipids, and Mg^{2+}, alongside various control reactions missing one of these essential components. Figure 3.11A shows that all components are required in the reaction mixture to produce a linear increase of the

phosphate concentration, which was determined by monitoring the absorbance at 620nm over time. The slope of these profiles, representing the rate of these reactions, was used to calculate the corresponding MinD activity values shown in Figure 3.11B. The complete reaction mixture showed a ~10 fold increase in the rate of ATP hydrolysis compared to the basal rate (No MinE), as previously observed for MinE-stimulated MinD activity (28, 30, 31).

Since MinD activity depends on the amount of MinE present, measurements of MinD-catalyzed ATP hydrolysis rates under a range of MinE concentrations can be fit to the Hill equation to obtain kinetic parameters that characterize the MinD-MinE interaction. An example of this type of analysis is shown in Figure 3.12 for MinD activity with WT MinE, giving rise to a sigmoidal plot with V_{max} of 58 nmol P_i/mgMinD•min, $K_{0.5}$ of 0.15 μM, and h of 1.6 in agreement with previously published values (31).

The kinetics of the MinE-MinD interaction with I24D was assessed to determine if the conformational transition from the 6-stranded to the 4-stranded form played a role in MinE-stimulated MinD ATPase activity. As shown in Figure 3.13, the profile for this mutant was very similar to that of WT MinE. As summarized in Table 3.4, the V_{max} and h values of this profile were essentially the same as that of WT MinE. However, the apparent affinity of I24D ($K_{0.5}$) was 0.22±0.04 μM, which was slightly higher than the WT. The similarity between these values and those of the WT indicate that the conformational exchange expected due to the introduction of a hydrophilic residue into the hydrophobic core does not have a large impact on the ability of MinE to interact with MinD.

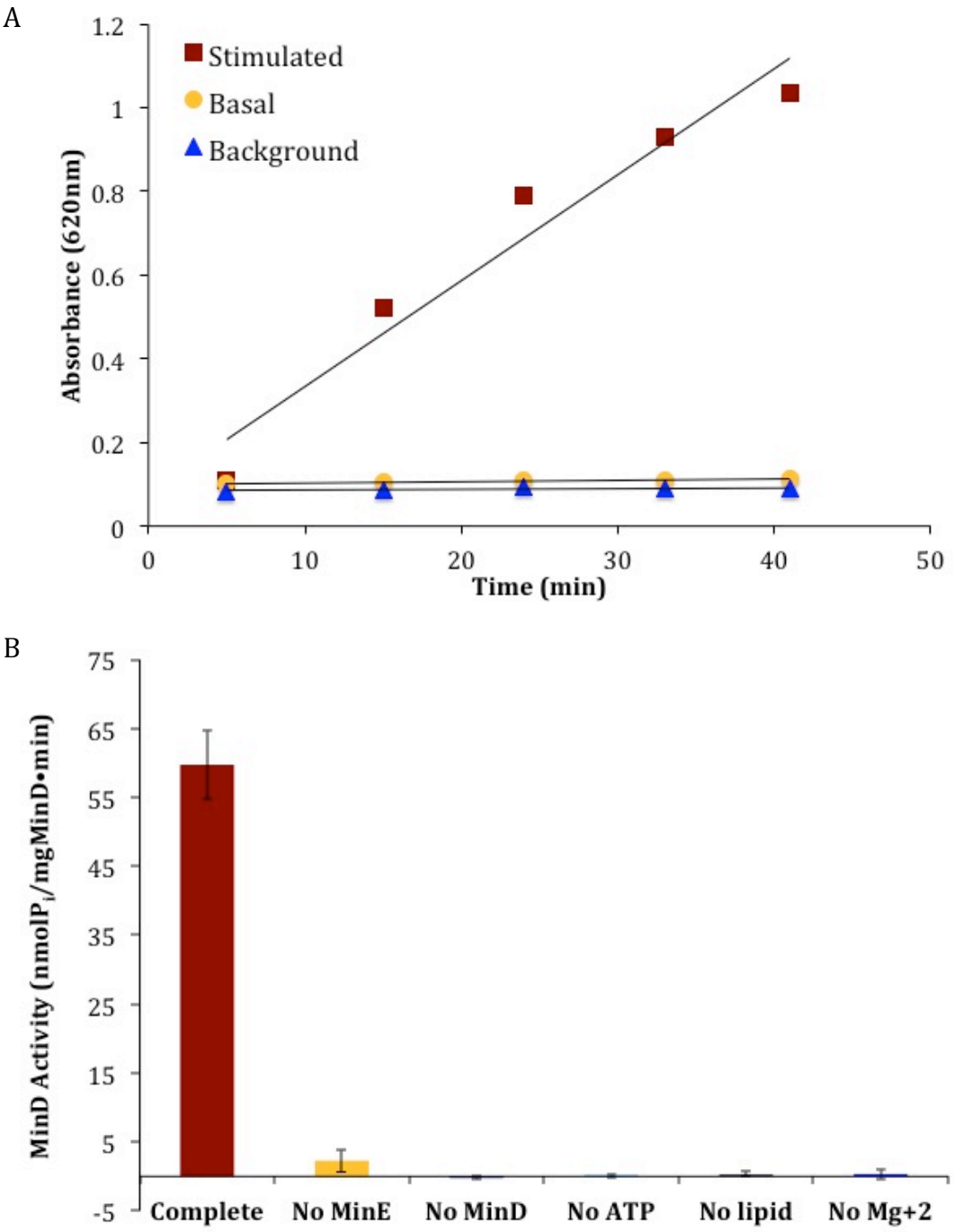

Figure 3.11: Example of rate measurement for MinE-stimulated MinD catalyzed ATP hydrolysis. A) Absorbance at 620 nm in a malachite green phosphate assay as a function of time for a complete reaction mixture (stimulated, red); a reaction mixture containing all components except for MinE (basal, yellow); and a reaction mixture missing either lipid vesicles, Mg^{2+} or ATP (background, blue). B) Slopes from absorbance vs. time plots were converted into ATP hydrolysis rates. All reactions contained 2.7 μM MinD and 1 μM MinE with the exceptions of the 'No MinD' and 'No MinE' controls respectively.

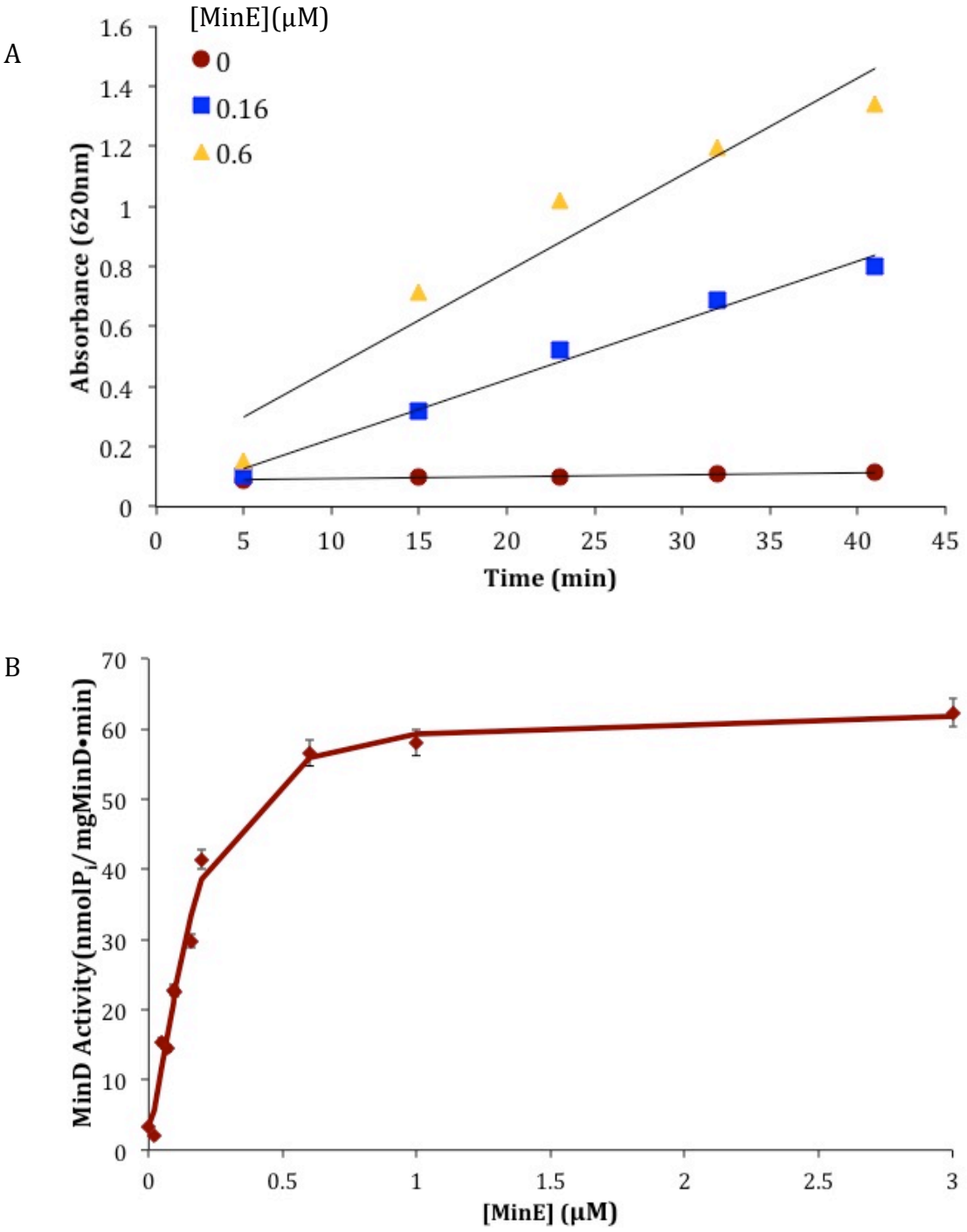

Figure 3.12: MinD activity as a function of MinE concentration. A) Sample of a MinD-catalyzed ATP hydrolysis rate measurement from absorbance at 620 nm vs. time plotted for a malachite green phosphate assay in the presence of indicated MinE concentration. B) Slope of absorbance plots from A) were converted into specific activity values and fit to the Hill equation to obtain parameters V_{Max} 58 nmolP_i/mgMinD•min, $K_{0.5}$ 0.15 μM, and h 1.6. Error bars were calculated as an average percent relative standard deviation between replicate runs at the same concentration.

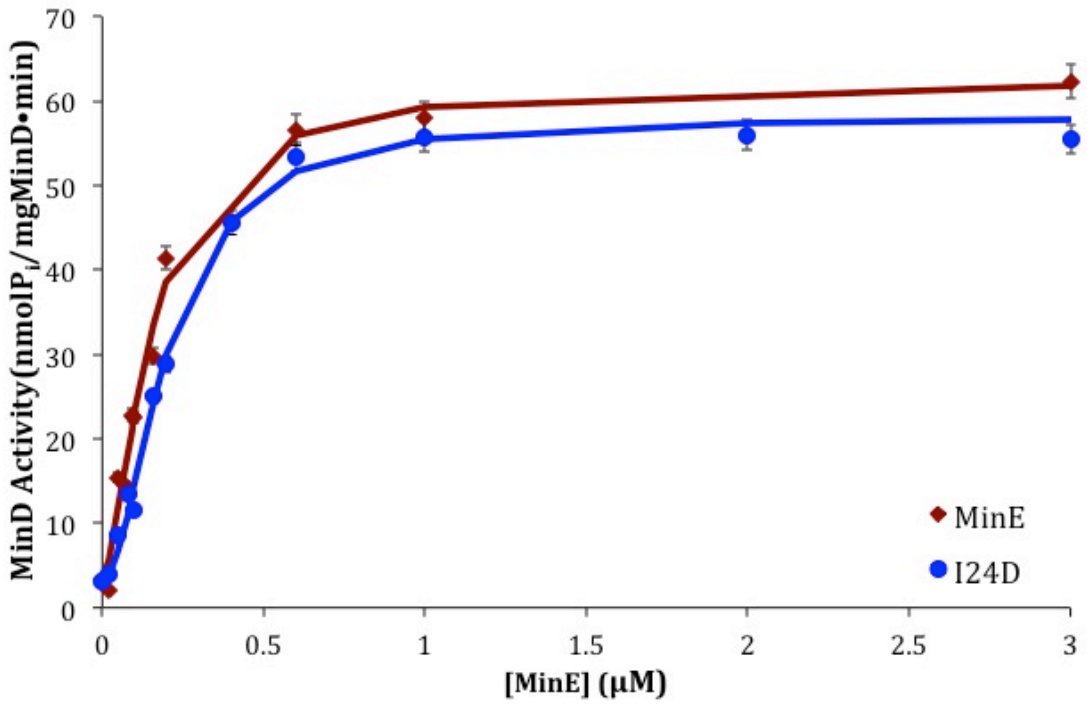

Figure 3.13: Overlay of representative kinetic profiles of MinD ATPase activity stimulated by either MinE (red) or I24D (blue). Theoretical curves, shown as solid lines, were obtained by fitting experimental data points to the Hill equation.

A peptide containing just the MinD-binding sequence (MinE12-30) was assessed for its ability to stimulate MinD activity to determine whether the lipid induced conformational change observed through CD plays a role in MinD stimulation by MinE. As shown in Figure 3.14, kinetic profiles obtained with this peptide were similar to that of the full-length protein, with comparable average V_{max} and h values (summarized in Table 3.4). $K_{0.5}$ was slightly higher for the peptide suggesting a small contribution of the MTS in the MinD interaction.

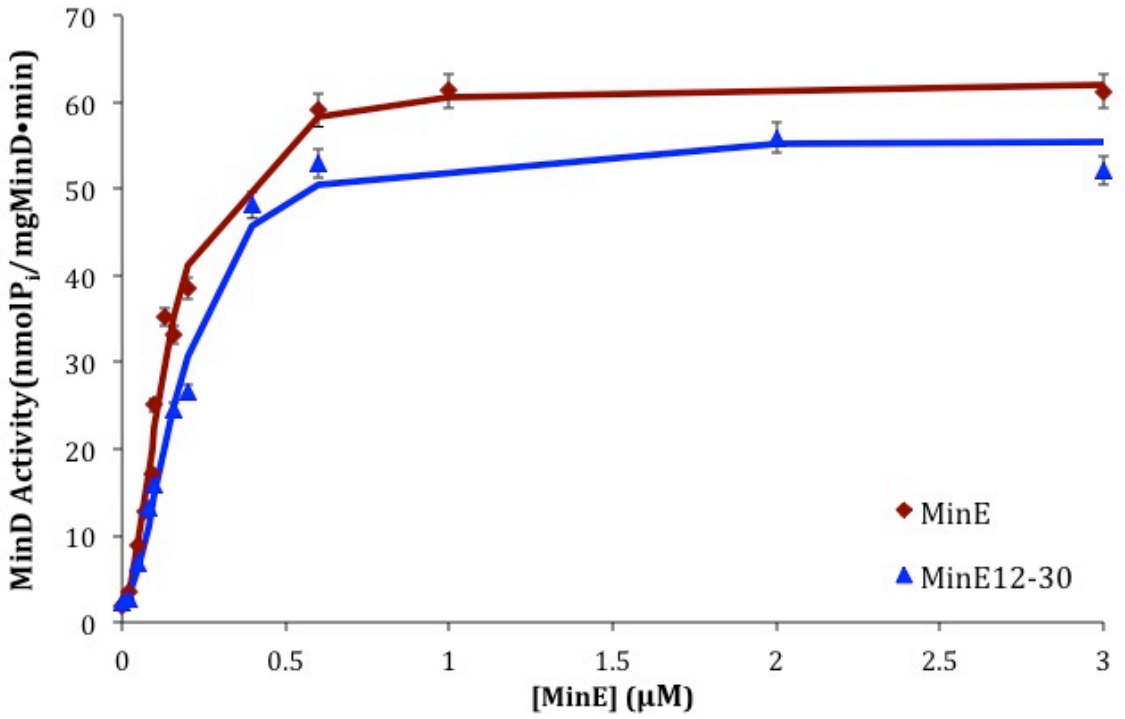

Figure 3.14: Activation of MinD-catalyzed ATP hydrolysis by MinE12-30.

Although the ATPase assay results with MinE12-30 suggest that MTS residues are not directly involved in MinD activation, the MTS may be required to induce conformational changes that could facilitate binding of the full-length protein. To address this issue, the two MinE truncation mutants missing the MTS, namely MinE12-87 and I24D12-87, were assessed for their ability to stimulate MinD ATPase activity. However, kinetic profiles for both MinE12-87 and I24D12-87 were indistinguishable from the WT profile (Fig. 3.15, Table 3.4). This data indicates that the conformational change required to pull out the MinD binding residues found in the dimeric interface of the 6-stranded structure can be achieved without the MTS-driven conformational change when the MTS is absent.

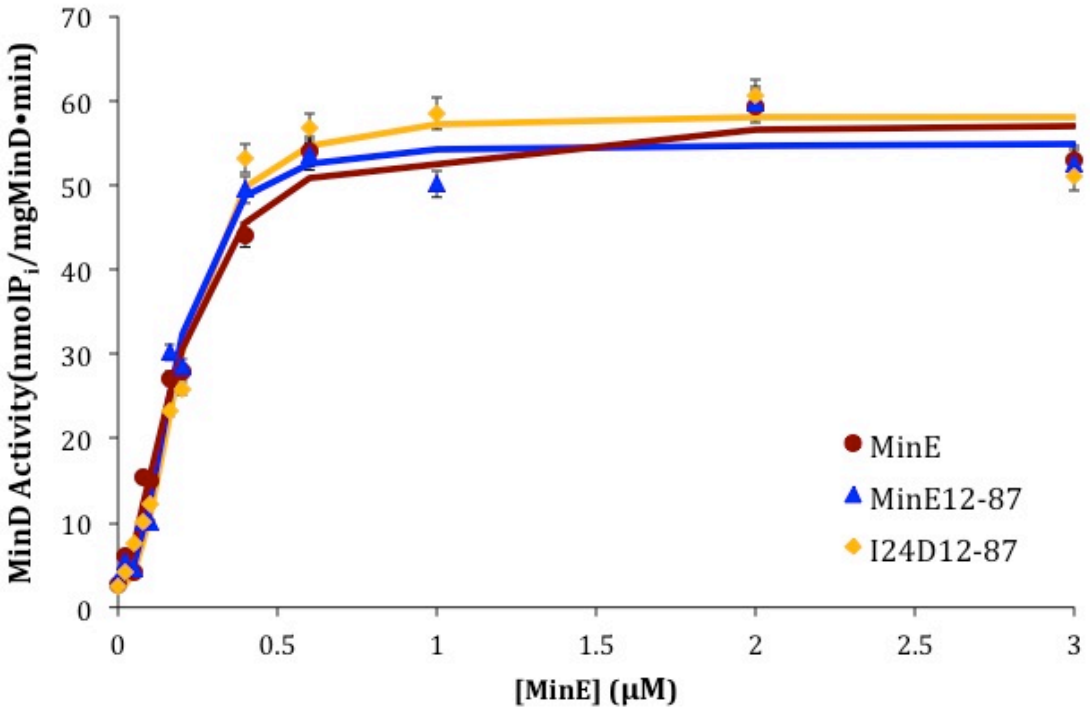

Figure 3.15: Kinetics profiles of MinE12-87 and I24D12-87 superimposed on the WT profile.

Table 3.4: Kinetic parameters of the MinD-MinE interaction with various MinE mutants and truncations. Values were obtained by measuring free phosphate production at a series of MinE concentrations and fitting values to the Hill equation.

	V_{max} (nmolP_i/mgMinD•min)	$K_{0.5}$ (μM)	h	n
WT	54±9	0.13±0.05	2.2±0.7	11
I24D	57±4	0.22±0.04	1.9±0.2	4
MinE12-30	58±4	0.24±0.05	2.0±0.2	4
MinE12-87	55±6	0.18±0.01	2.0±0.5	3
I24D12-87	53±4	0.18±0.03	2.2±0.4	2

3.8 Summary

The affinity of MinE for the membrane was measured with vesicles made from either DOPG or *E. coli* total lipid extracts. MinE was found to bind to DOPG lipids with almost 10-fold greater affinity, which is consistent with previous reports that MinE preferentially binds to negatively charged lipids (32, 62). These results also showed that the MTS is not required for MinD to gain access to binding residues of MinE under ATPase assay conditions suggesting that it may play a role in a part of the Min cycle not well represented in the assay.

Chapter 4: Discussion

4.1 Affinity of MinE for the Membrane

In this thesis, the affinity of MinE for lipid membranes was measured using LUVs comprised of either pure DOPG or *E. coli* total lipid extracts (Table 3.2). Dissociation constants measured here are ~50-fold greater than those previously reported on similar membrane systems (62). However, one of the reasons for this discrepancy may be due to the difference in techniques used. Specifically, previous experiments were carried out using planar bilayers deposited on a quartz crystal microbalance (QCM). Surprisingly, a range of lipid compositions, including those mimicking the composition of *E. coli* membranes, gave rise to a dissociation constant for MinE that was approximately the same as that for MinD (62). Those findings are difficult to reconcile with fluorescence microscopy studies demonstrating that MinD readily targets to the membrane periphery in the cell, while MinE remains largely cytoplasmic in the absence of MinD (14, 16). Moreover, independent localization of MinE to the membrane can only be induced *in vivo* if a mutation is introduced that would be expected to favor the 4-stranded conformation, such as I24N (33). This suggests that the QCM measurements that gave rise to the low K_d values for the MinE-membrane interaction may not be physiologically meaningful. This is supported by dissociation constants measured for MinD-membrane interactions, since the QCM-derived K_d values for MinD were also consistently lower than those measured by vesicle sedimentation (26). In contrast, our dissociation constants for the MinE-membrane interaction were at least 50-fold higher than those measured for MinD in comparable lipid systems using vesicle

sedimentation (26). The tendency of MinD to bind to the membrane with greater affinity than MinE is in agreement with *in vivo* localization studies where MinD was shown to target to the membrane independently while MinE did not (14, 16).

4.2 Co-operative Binding of MinE to Lipids

An interesting feature of the MinE interaction with lipids detected by CD, which had not been previously observed, was binding co-operativity (Table 3.2). Although this was evaluated in the QCM measurements, the Hill coefficient was found to be 1, indicating that MinE binding was not co-operative (62). A similar suggestion of non-cooperativity in binding also arose from studies of fluorescently tagged Min waves carried out on supported bilayers (19). Specifically, fluorescently labeled MinE was introduced into a standing wave created by fluorescently labeled MinD and unlabeled MinE on a planar lipid bilayer. The newly introduced MinE preferentially associated with the front of the wave, where MinE concentration was lowest, instead of at the back where it was the highest. Based on the high MinD density present through the bulk of the wave it is likely that the majority of these membrane association events arose from MinE interactions with membrane-bound MinD, and not a direct interaction between MinE and the membrane. However, the ability of MinE to persist on the membrane and collect at the trailing edge of the wave (19) as outlined in Chapters 1.3 and 1.4 suggests that direct interactions between MinE and the membrane could also be occurring at this point. Overall, the complexity of this system makes it difficult to separate binding contributions between MinE and MinD from those between MinE and the membrane. Nonetheless, given the presence of two MTS domains in each MinE dimer, it is logical to

expect that binding of one subunit to the membrane would promote binding of the other subunit to the membrane, even if only through a proximity effect. Therefore the co-operativity values measured by CD are reasonable for a dimeric system containing two membrane-binding domains.

4.3 Effect of Ionic Strength on the MinE-Membrane Interaction

In order to measure the affinity of MinE for membranes, it is necessary to use LUVs produced by extrusion (diameter ≥ 100 nm), since small unilamellar vesicles are metastable (63, 64) and have curvature that can alter protein-binding characteristics (65-69). However, CD spectra of solutions containing LUVs tend to suffer from light scattering effects that distort the spectrum, particularly below ~200 nm. Additional interference can also arise in this region due to strong absorbance from chloride ions that could prevent acquisition of distortion-free spectra when added to the scattering effects of the LUVs (45). Therefore to minimize these effects, we measured dissociation constants in the absence of salt. However, K_d values measured in the absence of salt may give rise to an overestimate of the strength of the MinE-membrane interaction *in vivo* or in the ATPase assay performed *in vitro*. This may be a significant factor since vesicle sedimentation studies showed that salt concentrations greater than 200 mM prevent detection of any interaction between MinE and the membrane (32). Nonetheless, CD spectra of MinE under conditions similar to *in vitro* assay conditions (i.e. 0.5 mg/mL DOPG, 130 mM NaCl), still showed a spectrum similar to the DOPG-bound state that was observed in the absence of salt (Figs. 3.6 and 3.8). In the future it would be useful to determine the dissociation constant between MinE and the

membrane under conditions that more precisely mimic those used in the MinD ATPase assay, potentially using other methods such as isothermal titration calorimetry (70, 71). This would permit a more accurate prediction of the proportion of MinE likely to be bound to lipids over the course of the assay.

4.4 How is the 4-Stranded Conformation Induced?

In this thesis, as well as in previous studies (33), structure-disrupting mutations were introduced into the Ile-24 position to induce a 4-stranded conformation in MinE. It is likely that the mutant studied in this work (I24D) would promote this conformation, since the MinE-I24N construct, which lacked 11 N-terminal residues, was 4-stranded in a crystal structure in complex with MinD (33). Since Ile-24 points into the hydrophobic core of the dimer interface in the structure of WT MinE, it is likely that the Asp mutation in this location would invoke similar structural disruptions. This was confirmed by deconvolution of CD spectra, which showed a decrease in the β-sheet content relative to that of full-length MinE (Table 3.3). I24D showed no change in helical content, indicating that the sheets became random coil upon removal from the dimer interface. These secondary structure changes are similar to those seen in CD studies of MinE and MinE-I24N constructs beginning at residue 21 (33).

A similar trend was also observed for the truncated MinE constructs, with the I24D truncation showing a significant decrease in sheet content relative to the WT truncation (Table 3.3). Somewhat unexpectedly, a significantly larger amount of helix was observed in I24D12-87 relative to the WT truncation, suggesting that while the 4-stranded conformation was induced, the liberated β-strands adopted a helical

conformation. One factor that may help to explain this apparent discrepancy between results for the full-length and truncation mutant is the difference in salt concentrations used. Under the increased salt concentrations used to mimic the ATPase assay I24D was soluble in the absence of lipid but would rapidly precipitate upon addition of 0.5 mg/mL DOPG. To facilitate comparison of spectra between lipid-bound and free states the I24D spectra were collected with 40 mM NaCl, a condition where both states could be maintained in solution. The lower salt concentration would have reduced electrostatic screening of interactions involving charged residues. This factor is likely important for a helical configuration such as that observed in the MinE-I24N structure in complex with MinD. As shown in Figure 4.1, the residues immediately above and below residue 24 in the helix are both negatively charged glutamic acids. With the added negative charge of the aspartic acid residue in the construct used in our work, the extra salt concentration may have been important to shield these charges, allowing the helix to form for the I24D12-87 mutant. In contrast, the electrostatic repulsion under the lower salt concentrations used for full-length I24D may have been significant enough to prevent helix formation, giving rise to a random coil signal in the spectrum. To test this hypothesis, future CD experiments could be done that monitor the effect of salt concentration on the I24D structure in the absence of lipid.

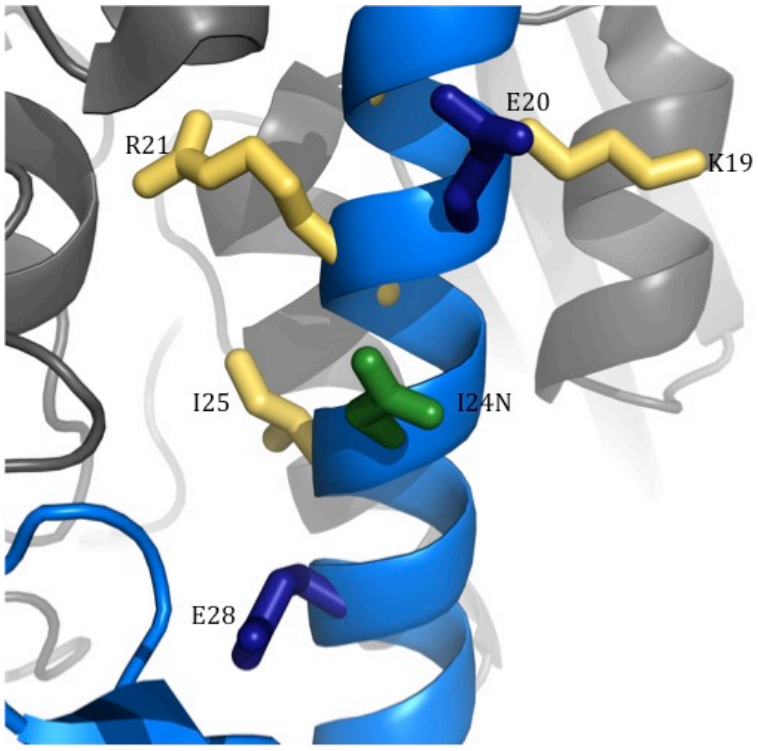

Figure 4.1: Negatively charged residues in close proximity to residue 24. Side chains of negatively charged Glu20 and Glu28 (blue) are shown with that of residue 24 (green). Side chains of MinD binding residues are also shown in yellow. PDB ID 3R9J (33)

As summarized in Table 3.3, lipid bound MinE shows a decrease in sheet content and increase in helix content relative to the lipid-free conformation. This pattern of structural change is consistent with the scenario where lipid binding converts the 6-stranded conformation into the 4-stranded state, with the freed sheet residues becoming helical, as was suggested by deconvolution of the I24D12-87 spectrum. This suggests that the conformational change required to free MinD binding residues could be achieved through lipid interaction. This is contrary to previous suggestions that the conformational change in MinE is entirely driven by interactions with MinD (33). Results from this study showed that the I24N mutation could rescue cell growth in division deficient mutants F7E or F3E, which were unable to target to the membrane or

grow on agar plates. This led to the conclusion that these residues were not only required for membrane binding but were also involved in a "sensing step" required to release the MTS before MinD-induced conformational change could occur (33). However, in the context of our study the rescue of the these MTS mutants by release of the central β-strands suggests that they were unable to undergo the membrane induced conformational change detected here, a step that does not require MinD (33).

Although the CD data suggest that membrane binding is sufficient to induce a 4-stranded conformation in MinE, it is important to note that the accuracy of secondary structure deconvolution from CD spectra is only on the order of ~70% (47, 72). This can be appreciated when comparing the secondary structure content obtained for full-length WT MinE (29% helix and 20% sheet, Table 3.3) to that found in the NMR structure (21% helix and 30% sheet, PDB2KXO)(31). A similar difference between expected secondary structure and that obtained by deconvolution of CD spectra was observed in measurements of MinE and MinE-I24N both truncated at residue 21 (33). However, the sensitivity of CD to the structural changes in MinE upon the addition of small amounts of lipid still make this a valuable tool to assess the structural impact of binding to a membrane surface. CD spectroscopy is also a useful method for the comparison of structures for related proteins, such as the WT and mutant proteins used in this study.

While CD spectroscopy was useful in the current study, higher resolution structural data, such as that provided by solution NMR, could provide a more detailed understanding of the relationship between the membrane-bound and MinD-bound structures. This type of information could help to elucidate the role of membrane

induced conformational change in MinE function. If the conformation induced by the membrane were the same as that required for MinD interaction, it would suggest that the role of membrane binding is to promote the 4-stranded conformation of MinE. This may have implications in the rapid rebinding model of Min wave propagation where MinE interacts with multiple MinD binding partners before dissociation from the wave. If the MTS can promote the 4-stranded structure it might provide MinE with a greater opportunity to find a MinD binding partner before dissociating from the membrane.

4.5 Functional Role of the MTS

Based on the comparison of CD spectra between I24D and WT MinE constructs, it appears that the MTS-membrane interaction may be required to induce the 4-stranded conformation of MinE. However, according to the kinetic profiles measured in this thesis, mutation induced change from the 6- to 4-stranded structure does not give rise to any change in the ability of MinE to stimulate MinD-catalyzed ATP hydrolysis (Fig. 3.13). Although the availability of a freely accessible anti-MinCD domain in the absence of lipids might be expected to provide some advantage for the MinDE interaction, no change in $K_{0.5}$ was observed for the I24D mutant (Table 3.4). However, according to dissociation constants measured in this thesis under assay conditions, the majority of WT MinE would be expected to be associated with the membrane. Since the membrane bound conformation of WT MinE is expected to be the same as that of the I24D mutant, no difference should be expected under the assay conditions used. While the assays were conducted with high lipid concentrations to allow direct comparison with previous measurements performed with this system (31), in the future it would be

useful to carry out the assay under conditions where a smaller proportion of WT MinE would be bound to the vesicles. This could be achieved by either reducing the concentration of vesicles, or using LUVs made from *E. coli* lipid extracts in place of DOPG.

Since our data suggested that membrane binding induces a conformational change in MinE that should facilitate the interaction between MinD and MinE, we expected that MinE12-87, a mutant that did not show any CD spectral changes upon addition of DOPG, would be inactive. Therefore, it was surprising to see that the ability of this mutant to stimulate MinD-catalyzed ATP hydrolysis was virtually indistinguishable from that of full-length MinE (Fig. 3.15, Table 3.4). Nonetheless, our results are consistent with rudimentary rate measurements performed on the C1 mutant, which was also defective in membrane binding (32). These results are particularly surprising given that ATP hydrolysis is considered to supply the source of energy for Min protein oscillation. Evidence for the central role of ATP hydrolysis has been provided by a number of results, such as the observation that standing Min waves on planar bilayers do not form in the presence of an unhydrolyzable ATP analogue (18). Furthermore, *in vivo* studies of MinE mutants deficient in MinD stimulation showed an altered rate of oscillation, providing another link between oscillation and ATP hydrolysis (30). However, ATP hydrolysis rates only reflect one aspect of MinE function, and therefore it is possible that some other facet of the Min system, not reflected by our ATP hydrolysis rate measurements, is altered by loss of direct MinE-membrane interaction.

One feature of Min protein function that may be altered by the loss of membrane-binding affinity is the pattern of Min protein localization. Some support for this idea is provided by observations of aberrant pattern formation by the lipid binding-defective C1 mutant of MinE on planar lipid bilayers (19, 32). Fluorescently-labeled Min proteins did not form their characteristic pattern of waves on these bilayers, but instead remained in a semi-organized state generally observed in the early stages of wave development (19). This indicated that N-terminal basic residues might play a role in the establishment of the dynamic mesoscale and subcellular structures formed by the Min system. In addition, cross-sectional fluorescence profiles of these waves showed that MinE and MinD organization was similar to what is observed in parallel waves, with the crest of the MinD wave occurring slightly before that of MinE. In the case of WT MinE, this profile shows a spike in MinE intensity just prior to rapid dissociation from the membrane that occurs just after MinC is displaced from MinD. However, this peak is not observed with the C1 mutation. This indicates that the affinity of MinE for the membrane may be critical for the concerted disassembly of Min proteins from the bilayer surface.

While it was assumed that the C1 mutant was entirely unable to bind to the membrane in these fluorescence microscopy studies, it should be noted that hydrophobic residues remained in the N-terminal MTS (19, 33) and therefore some interaction between MinE and the membrane may have been possible. This could provide an explanation for the residual organization that was observed in this system (19). For this reason, it would be useful to quantify the membrane binding affinity for the C1 mutant in the future, to determine the extent to which membrane binding was

actually abolished by the substitution of 3 basic residues for negatively charged residues. In addition, future study of fluorescently tagged variants of our truncation mutants, either *in vivo* or in a planar wave system, would provide valuable insight into the role of the MTS in the organization of the Min system.

Another interesting feature of the C1 mutant that may be relevant for MTS function is that it was not able to displace MinC from the MinCD complex (19). This suggests that the affinity of MinE for MinD might be enhanced by the interactions between the membrane and the MTS. Although the ATPase assay used in this thesis suggested no significant differences in the apparent affinity of MinE for MinD upon truncation of the MTS in either the 6- or 4-stranded conformation (Table 3.4), it is possible that the actual affinity was altered but not detected in our assay.

To better understand potential differences in binding behavior of our mutants, it would be valuable to quantify binding affinity for both the membrane and MinD using more direct methods. For example, it is possible to fix a lipid bilayer to a chip used in surface plasmon resonance measurements (73). In this case, the membrane could first be saturated with a hydrolysis-deficient MinD mutant such as D40A (29) bound to ATP. Then, MinE could be allowed to flow over this surface to study the kinetics and affinity of association. This measurement could also be performed in the absence of MinD, and with MinD concentrations that do not saturate the membrane. Taken together, this data could provide new insights into the interaction between MinE and the MinD-lipid surface, closer to the conditions it might encounter *in vivo*. In addition, this more direct analysis may help to determine the function of the conformational transition between the 6-stranded and 4-stranded forms of MinE. Ultimately, these studies may provide

insight into some of the observations made in the study of dynamic pattern formation by Min proteins, such as the tendency of MinE to enter the front of a standing Min wave and to persist on the membrane during wave propagation (19).

4.6 Redundancy in the Min Reaction Cycle

Based on the results presented in this thesis some changes to the Min reaction cycle model (Fig. 1.4) can be made with regards to the mechanism by which MinE interacts with MinD (Fig. 4.2). Secondary structure deconvolution of the MinE-lipid bound CD spectra suggest that the conformational change from the 6-stranded to 4-stranded structure is mediated by lipid interaction (Table 3.3). These results indicate that MinD binding could occur through a two step process with MinE first binding the lipid membrane (step 2a), exposing MinD binding residues, then interacting with MinD (step 2b). However, the ability of MinE12-87 to stimulate the ATPase activity of MinD as effectively as WT MinE (Table 3.4), while being unable to undergo membrane-induced conformational change, indicates that it is also possible for MinD to mediate the transition from the 6-stranded to 4-stranded structure in the absence of membrane-mediated conformational change (step 3). Taken together this suggests that there are two pathways MinE can take to interact with MinD, with either 2-steps involving the membrane and MinD or 1-step involving only MinD. These alternative pathways may also be available in the dissociation of the MinDE complex. MinE may either dissociate from MinD but remain bound to the membrane (step 4a), available for interaction with an adjacent MinD (step 6), as has been previously suggested (33), or dissociate from both MinD and the membrane and become cytoplasmic (step 5). These

redundant pathways may play a role in ability of MinE to accumulate at the rear of standing Min waves (19). If both MinD and the membrane are able to mediate the transition from the 6-stranded to 4-stranded conformation then both cytoplasmic and membrane bound MinE can be incorporated into traveling Min waves. The introduction of fluorescently labeled MinE into waves of labeled MinD and unlabeled MinE showed that MinE preferentially enters the wave at the leading edge, where MinD density is low (19). At low MinD density more lipid would be exposed so MinE could be taking the 2-step pathway. If MinE dissociated from the wave before reaching the trailing edge the 1-step path could be taken to reincorporate it into the wave without requiring that molecule to begin again at the front of the wave. The redundant nature of these two pathways may allow MinE to accumulate more quickly at the rear of the wave, which could influence the timing of the concerted dissociation of Min proteins required for proper oscillation (19).

4.7 Concluding Remarks

The work carried out in this thesis aimed to characterize the lipid induced conformational change of the MinE structure observed through CD. While affinity measurements have provided some insight into Min protein behavior on the membrane, many questions remain with regards to the function of the MTS of MinE. Truncations demonstrated that the conformational change induced by membrane interaction is not required to allow MinD to gain access to binding residues on MinE. However, it is very likely that the MTS plays a significant role in the large-scale organization of the Min system, although the details of this role are still poorly

understood. The Min system, while being one of the simplest examples of dynamic pattern formation, is still amazingly complex. Deeper understanding of this system will help to model dynamics in other, higher order systems, and also help to identify means through which it can be inhibited as a future antibiotic target.

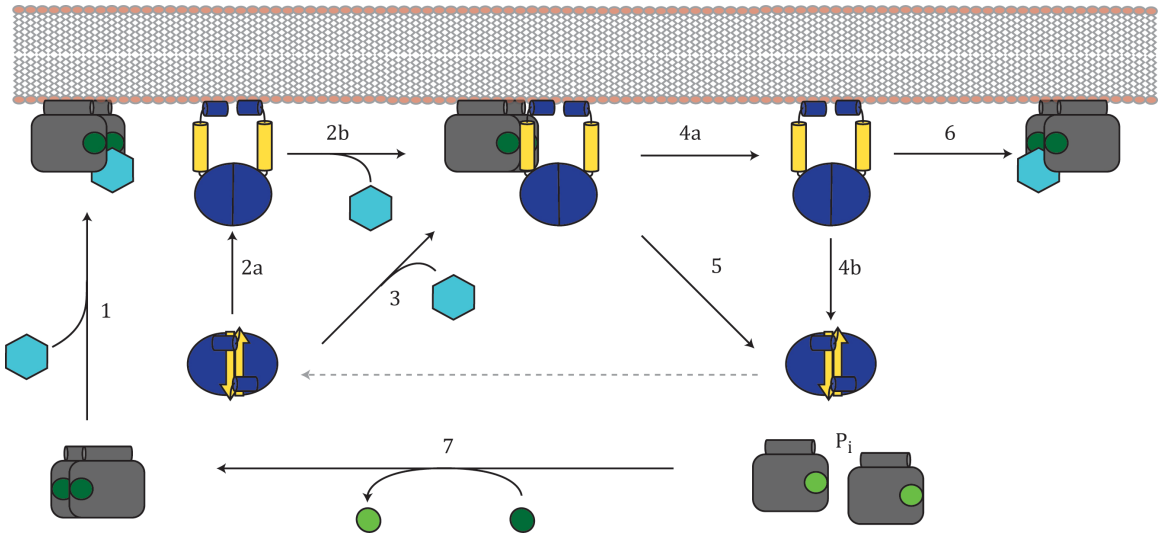

Figure 4.2: Redundancy in the Min reaction cycle. Dimeric, ATP-bound MinD (grey square, dark green circle) targets to the interior of the cell membrane where it interacts with MinC (light blue hexagon) (step 1). MinE (dark blue oval) can interact with MinD through either a two-step mechanism where it interacts first with the membrane (step 2a) and then with MinD (step 2b) or through a direct mechanism from the cytoplasm (step 3). In both cases interaction between MinD and MinE causes displacement of MinC. Once bound MinE stimulates the ATPase activity of MinD. After simulation MinE either becomes cytoplasmic (step 5) or remains bound to the membrane (step 4a), where it can then become cytoplasmic (step 4b) or interact with a nearby MinD on the membrane (step 6). In either scenario MinD dissociates from the membrane upon hydrolysis of ATP (grey square, light green circle) (steps 4a and 5). Nucleotide exchange must take place before MinD can retarget to the membrane (step 7). MinE can re-enter the cycle in its cytoplasmic form (grey dashed line). (9)

References

1. Fleming A (1929) On the antibacterial action of cultures of a penicillium, with special reference to their use in the isolation of B. influenzae*. The British Journal of Experimental Pathology* 10:226-236

2. Martin I et al. (2012) Emergence and characterization of *Neisseria gonorrhoeae* isolates with decreased susceptibilities to ceftriaxone and cefixime in Canada: 2001-2010. *Sexually Transmitted Diseases* 39:316–323.

3. Ontario Agency for Health Protection and Promotion (Public Health Ontario). Guidelines for testing and treatment of gonorrhea in Ontario. Toronto, ON: Queen's Printer for Ontario; 2013.

4. Ramirez-Arcos S et al. (2001) Deletion of the cell-division inhibitor MinC results in lysis of *Neisseria gonorrhoeae*. *Microbiology* 147:225-237

5. Lutkenhaus J and Addinall SG (1997) Bacterial cell division and the Z ring. *Annual Reviews of Biochemistry*. 66:93-116

6. Buddelmeijer N, Beckwith J (2002) Assembly of cell division proteins at the *E. coli* cell center. *Current Opinion in Microbiology* 5:553–557.

7. Wu LJ, Errington J (2011) Nucleoid occlusion and bacterial cell division. *Nature Reviews Microbiology* 10:8–12.

8. de Boer PAJ, Crossley RE, Rothfield LI (1989) A division inhibitor and a topological specificity factor coded for by the minicell locus determine proper placement of the division septum in *E. coli*. *Cell* 56:641–649.

9. Lutkenhaus J (2007) Assembly dynamics of the bacterial MinCDE system and spatial regulation of the Z ring. *Annual Reviews of Biochemistry* 76:539–562.

10. Raskin DM, de Boer PAJ (1999) MinDE-Dependent Pole-to-Pole Oscillation of Division Inhibitor MinC in Escherichia coli. *Journal of Bacteriology*. 181: 6419-6424

11. Hu Z, Lutkenhaus J (1999) Topological regulation of cell division in Escherichia coli involves rapid pole to pole oscillation of the division inhibitor MinC under the control of MinD and MinE. *Molecular Microbiology* 34:82–90.

12. Hu Z, Lutkenhaus J (2000) Analysis of MinC reveals two independent domains involved in interaction with MinD and FtsZ. *Journal of Bacteriology* 182:3965–3971.

13. Hu Z, Mukherjee A, Pichoff S, Lutkenhaus J (1999) The MinC component of the division site selection system in Escherichia coli interacts with FtsZ to prevent polymerization. *Proceedings of the National Academy of Sciences USA* 96:14819–14824.

14. Raskin DM, de Boer PAJ (1999) Rapid pole-to-pole oscillation of a protein required for directing division to the middle of Escherichia coli. *Proceedings of the National Academy of Sciences USA* 96:4971–4976.

15. Hale CA, Meinhardt H, de Boer PAJ (2001) Dynamic localization cycle of the cell division regulator MinE in Escherichia coli. *EMBO J* 20:1563–1572.

16. Raskin DM, de Boer PA (1997) The MinE ring: an FtsZ-independent cell structure required for selection of the correct division site in *E. coli*. *Cell* 91:685–694.

17. Shih Y-L, Le T, Rothfield L (2003) Division site selection in Escherichia coli involves dynamic redistribution of Min proteins within coiled structures that extend between the two cell poles. *Proceedings of the National Academy of Sciences USA* 100:7865–7870.

18. Loose M, Fischer-Friedrich E, Ries J, Kruse K, Schwille P (2008) Spatial regulators for bacterial cell division self-organize into surface waves *in vitro*. *Science* 320:789–792.

19. Loose M, Fischer-Friedrich E, Herold C, Kruse K, Schwille P (2011) Min protein patterns emerge from rapid rebinding and membrane interaction of MinE. *Nature Structural and Molecular Biology* 18:577–583.

20. Lutkenhaus J, Sundaramoorthy M (2003) MinD and role of the deviant Walker A motif, dimerization and membrane binding in oscillation. *Molecular Microbiology* 48:295–303.

21. Hu Z, Saez C, Lutkenhaus J (2003) Recruitment of MinC, an inhibitor of Z-ring formation, to the membrane in Escherichia coli: role of MinD and MinE. *Journal of Bacteriology* 185:196–203.

22. Szeto J et al. (2001) Gonococcal MinD affects cell division in *Neisseria gonorrhoeae* and Escherichia coli and exhibits a novel self-interaction. *Journal of Bacteriology* 183:6253–6264.

23. Hu Z, Lutkenhaus J (2003) A conserved sequence at the C-terminus of MinD is required for binding to the membrane and targeting MinC to the septum. *Molecular Microbiology* 47:345–355.

24. Szeto TH, Rowland SL, Rothfield LI, King GF (2002) Membrane localization of MinD is mediated by a C-terminal motif that is conserved across eubacteria, archaea, and chloroplasts. *Proceedings of the National Academy of Sciences USA* 99:15693–15698.

25. Taghbalout A, Ma L, Rothfield L (2006) Role Of MinD-Membrane Association in Min Protein Interactions. *Journal of Bacteriology* 188:2993–3001.

26. Mileykovskaya E et al. (2003) Effects of phospholipid composition on MinD-membrane interactions *in vitro* and *in vivo*. *Journal of Biological Chemistry* 278:22193–22198.

27. Hu Z, Gogol EP, Lutkenhaus J (2002) Dynamic assembly of MinD on phospholipid vesicles regulated by ATP and MinE. *Proceedings of the National Academy of Sciences USA* 99:6761–6766.

28. Lackner LL, Raskin DM, de Boer PAJ (2003) ATP-Dependent Interactions between Escherichia coli Min Proteins and the Phospholipid Membrane *In Vitro*. *Journal of Bacteriology* 185:735-749

29. Wu W, Park K-T, Holyoak T, Lutkenhaus J (2011) Determination of the structure of the MinD-ATP complex reveals the orientation of MinD on the membrane and the relative location of the binding sites for MinE and MinC. *Molecular Microbiology* 79:1515–1528.

30. Hu Z, Lutkenhaus J (2001) Topological regulation of cell division in *E. coli*: spatiotemporal oscillation of MinD requires stimulation of its ATPase by MinE and phospholipid. *Molecular Cell* 7:1337–1343.

31. Ghasriani H et al. (2010) Appropriation of the MinD protein-interaction motif by the dimeric interface of the bacterial cell division regulator MinE. *Proceedings of the National Academy of Sciences USA* 107:18416–18421.

32. Hsieh C-W et al. (2010) Direct MinE-membrane interaction contributes to the proper localization of MinDE in *E. coli*. *Molecular Microbiology* 75:499–512.

33. Park K-T et al. (2011) The Min Oscillator Uses MinD-Dependent Conformational Changes in MinE to Spatially Regulate Cytokinesis. *Cell* 146:396–407.

34. Altschul SF et al. (2005) Protein database searches using compositionally adjusted substitution matrices. *FEBS J* 272:5101–5109.

35. Altschul SF et al. (1997) Gapped BLAST and PSI-BLAST: a new generation of protein database search programs. *Nucleic Acids Research* 25:3389–3402.

36. Ramirez-Arcos S, Szeto J, Dillon J-AR, Margolin W (2002) Conservation of dynamic localization among MinD and MinE orthologues: oscillation of *Neisseria gonorrhoeae* proteins in Escherichia coli. *Molecular Microbiology* 46:493–504.

37. Zhao CR, de Boer PAJ, Rothfield LI (1995) Proper placement of the Escherichia coli division site requires two functions that are associated with different domains of the MinE protein. *Proceedings of the National Academy of Sciences USA* 92:4313–4317.

38. Ma L-Y, King G, Rothfield L (2003) Mapping the MinE site involved in interaction with the MinD division site selection protein of Escherichia coli. *J Bacteriol* 185:4948–4955.

39. King GF et al. (2000) Structural basis for the topological specificity function of MinE. *Nature Structural Biology* 7:1013–1017.

40. King GF et al. (1999) The dimerization and topological specificity functions of MinE reside in a structurally autonomous C-terminal domain. *Molecular Microbiology* 31:1161–1169.

41. Ramos D et al. (2006) Conformation of the cell division regulator MinE: evidence for interactions between the topological specificity and anti-MinCD domains. *Biochemistry* 45:4593–4601.

42. McLeod L (2010) Investigation of the Role of the Dimeric State of Bacterial Cell Division Regulator MinE. Honours Thesis, University of Ottawa

43. Hafizi F (2012) Characterization of the Interactions of the Bacterial Cell Division Regulator MinE. Masters Thesis, University of Ottawa

44. Greenfield NJ (2007) Using circular dichroism spectra to estimate protein secondary structure. *Nature Protocols* 1:2876–2890.

45. Kelly SM, Jess TJ, Price NC (2005) How to study proteins by circular dichroism. *Biochimica et Biophysica Acta* 1751:119–139.

46. Sreerama N, Woody RW (1993) A self-consistent method for the analysis of protein secondary structure from circular dichroism. *Analytical Biochemistry* 209:32–44.

47. Sreerama N, Woody RW (2000) Estimation of protein secondary structure from circular dichroism spectra: comparison of CONTIN, SELCON, and CDSSTR methods with an expanded reference set. *Analytical Biochemistry* 287:252–260.

48. Johnson WC (1999) Analyzing protein circular dichroism spectra for accurate secondary structures. *Proteins* 35:307–312.

49. Provencher SW, Glöckner J (1981) Estimation of globular protein secondary structure from circular dichroism. *Biochemistry* 20:33–37.

50. Voet D, Voet JG (2004) *Biochemistry, 3rd Edition.* John Wiley & Sons.

51. Weiss JN (1997) The Hill equation revisited: uses and misuses. *FASEB J* 11:835–841.

52. Hill AV (1910) The combinations of haemoglobin with oxygen and with carbon monoxide and oxygen. *The Journal of Physiology* 40:iv-vii

53. Sambrook J, Fritsch EF, Maniatis T (1989) *Molecular cloning: A laboratory manual.* Cold Spring Harbor Laboratory Press, Cold Spring Harbor, New York

54. Bertani G (1951) Studies on lysogenesis. I. The mode of phage liberation by lysogenic Escherichia coli. *Journal of Bacteriology* 62:293–300.

55. Eng NF, Szeto J, Acharya S, Tessier D, Dillon J-AR (2006) The C-terminus of MinE from *Neisseria gonorrhoeae* acts as a topological specificity factor by modulating MinD activity in bacterial cell division. *Research in Microbiology* 157:333–344.

56. Ford KG, Whitmarsh AJ, Hornby DP (1994) Overexpression and purification of eukaryotic transcription factors as glutathione-S-transferase fusions in *E. coli. Methods in Molecular Biology* 30:185–197.

57. Wiechelman KJ, Braun RD, Fitzpatrick JD (1988) Investigation of the bicinchoninic acid protein assay: Identification of the groups responsible for color formation. *Analytical Biochemistry* 175:231–237.

58. Smith PK et al. (1985) Measurement of protein using bicinchoninic acid. *Analytical Biochemistry* 150:76-86

59. Feng J et al. (2011) An improved malachite green assay of phosphate: Mechanism and application. *Analytical Biochemistry* 409:144–149.

60. K W Harder et al. (1994) Characterization and kinetic analysis of the intracellular domain of human protein tyrosine phosphatase beta (HPTP beta) using synthetic phosphopeptides. *Biochemical Journal* 298:395-401

61. Geladopoulos TP, Sotiroudis TG, Evangelopoulos AE (1991) A malachite green colorimetric assay for protein phosphatase activity. *Analytical Biochemistry* 192:112–116.

62. Renner LD, Weibel DB (2012) MinD and MinE Interact with Anionic Phospholipids and Regulate Division Plane Formation in Escherichia coli. *Journal of Biological Chemistry* 287:38835–38844.

63. Wong M, Anthony FH, Tillack TW, Thompson TE (1982) Fusion of dipalmitoylphosphatidylcholine vesicles at 4 degrees C. *Biochemistry* 21:4126–4132.

64. Schmidt CF, Lichtenberg D, Thompson TE (1981) Vesicle-vesicle interactions in sonicated dispersions of dipalmitoylphosphatidylcholine. *Biochemistry* 20:4792-4797

65. Ladokhin AS, Fernández-Vidal M, White SH (2010) CD spectroscopy of peptides and proteins bound to large unilamellar vesicles. *Journal of Membrane Biology* 236:247–253.

66. Ladokhin AS, Jayasinghe S, White SH (2000) How to measure and analyze tryptophan fluorescence in membranes properly, and why bother? *Analytical Biochemistry* 285:235–245.

67. Seelig J, Ganz P (1991) Nonclassical hydrophobic effect in membrane binding equilibria. *Biochemistry* 30:9354–9359.

68. Greenhut SF, Bourgeois VR, Roseman MA (1986) Distribution of cytochrome b5 between small and large unilamellar phospholipid vesicles. *Journal of Biological Chemistry* 261:3670–3675.

69. Plager DA, Nelsestuen GL (1994) Direct enthalpy measurements of factor X and prothrombin association with small and large unilamellar vesicles. *Biochemistry* 33:7005–7013.

70. Doyle ML (1997) Characterization of binding interactions by isothermal titration calorimetry. *Current Opinion in Biotechnology* 8:31–35.

71. Pierce MM, Raman CS, Nall BT (1999) Isothermal titration calorimetry of protein-protein interactions. *Methods* 19:213-221

72. Rost B, Sander C (1993) Prediction of protein secondary structure at better than 70% accuracy. *Journal of Molecular Biology* 232:584-599

73. Pattnaik P (2005) Surface Plasmon Resonance: Applications in Understanding Receptor–Ligand Interaction. *Applied Biochemistry and Biotechnology* 126:079–092.

Appendix

A.1 Tables

Table A1: Translated sequencing results from mutagenesis reactions carried out to create N terminal truncations in MinE and I24D plasmids

Protein	Translated Sequencing Result
MinE	MSLIELLFGR KQKTATVARD RLQIIIAQER AQEGQTPDYL PTLRKELMEV LSKYVNVSLD NIRISQEKQD GMDVLELNIT LPEQKKVLEH HHHHH
MinE6-87	MLFGRKQKTA TVARDRLQII IAQERAQEGQ TPDYLPTLRK ELMEVLSKYV NVSLDNIRIS QEKQDGMDVL ELNITLPEQK KVLEHHHHHH
I24D6-87	MLFGRKQKTA TVARDRLQDI IAQERAQEGQ TPDYLPTLRK ELMEVLSKYV NVSLDNIRIS QEKQDGMDVL ELNITLPEQK KVLEHHHHHH
MinE12-87	MQKTATVARD RLQIIIAQER AQEGQTPDYL PTLRKELMEV LSKYVNVSLD NIRISQEKQD GMDVLELNIT LPEQKKVLEH HHHHH
I24D12-87	MQKTATVARD RLQDIIAQER AQEGQTPDYL PTLRKELMEV LSKYVNVSLD NIRISQEKQD GMDVLELNIT LPEQKKVLEH HHHHH

Table A2: P values associated with t-tests comparing secondary structure compositions determined by CD deconvolution. T-tests were carried out to determine statistical significance of differences in secondary structure percentages obtained through deconvolution of CD spectra. Lipids were DOPG except where marked with an asterisk.

Protein		MinE				I24D		MinE12-87		I24D12-87	
[lipid]		0.5	0.5*	0	0.5	0	0.5	0	0.5	0	0.5
[NaCl]		0	0	130	130	40	40	130	130	130	130
MinE 0, 0	α	1.5E-12	6.4E-11	4.1E-02	4.1E-05	6.1E-01	2.2E-12	1.9E-09	3.0E-02	7.1E-07	1.5E-07
	β	2.4E-11	1.7E-09	3.6E-01	1.4E-04	8.9E-05	9.3E-13	1.5E-01	6.0E-01	9.5E-11	1.2E-11
MinE 0.5, 0	α		6.7E-02	7.2E-10	7.4E-04	4.9E-08	9.4E-01	1.3E-13	6.8E-08	1.8E-04	2.0E-04
	β		2.8E-01	9.4E-08	8.7E-03	2.1E-02	6.5E-02	1.6E-06	5.0E-05	9.6E-01	7.4E-01
I24D 0, 40	α						9.3E-12	2.5E-12	3.9E-02	9.6E-07	2.1E-08
	β						6.4E-04	2.3E-03	3.2E-02	3.2E-02	1.4E-02
I24D 0.5, 40	α							6.6E-16	1.2E-07	4.6E-06	1.8E-06
	β							1.1E-06	1.0E-05	7.6E-02	1.4E-01
MinE 12-87 0, 130	α								8.7E-03	3.3E-16	6.8E-18
	β								2.5E-01	1.5E-06	5.6E-07
MinE 12-87 0.5, 130	α									5.8E-06	2.1E-06
	β									9.9E-05	3.7E-05
I24D 12-87 0, 130	α										7.7E-01
	β										7.2E-01

*_E. coli_ total lipid extract

α = α-helix

β = β-sheet

A.2 Reprint Permissions

Figure 1.1 Reprinted from *Cell,* 56, de Boer PAJ, Crossley RE, Rothfield LI, A division inhibitor and a topological specificity factor coded for by the minicell locus determine proper placement of the division septum in *E. coli*, 641–649 Copyright (1989) with permission from Elsevier

Figure 1.2
Reprinted by permission from Standford University's Highwire Press: *Proceedings of the National Academy of Sciences USA,* 96:4971–4976, Raskin DM, de Boer PAJ (1999) Rapid pole-to-pole oscillation of a protein required for directing division to the middle of Escherichia coli, copyright 1999

Figure 1.3
Reprinted by permission from Macmillan Publishers Ltd: *Nature Structural and Molecular Biology* 18:577–583, Loose M, Fischer-Friedrich E, Herold C, Kruse K, Schwille P (2011) Min protein patterns emerge from rapid rebinding and membrane interaction of MinE, copyright 2011

Figure 1.10
Reprinted by permission from Macmillan Publishers Ltd: *Nature Protocols* Greenfield NJ, 1:2876–2890, (2007) Using circular dichroism spectra to estimate protein secondary structure, copyright 2007